AD-A184 725 UNSTEADY FLOW ABOUT CAMBERED PLATES(U) NAVAL POSTGRADUATE SCHOOL MONTEREY CA P D MUNZ JUN 87 1/1

UNCLASSIFIED F/G 20/4 NL

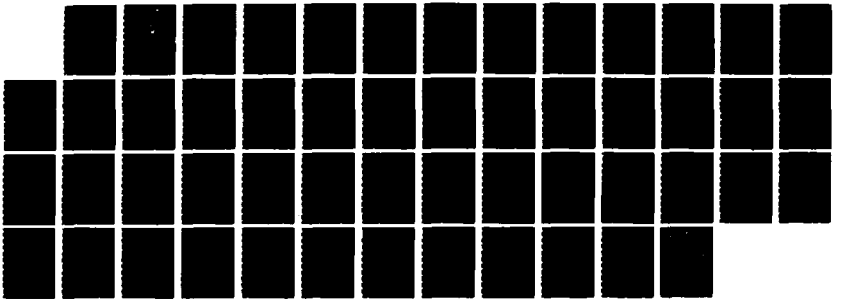

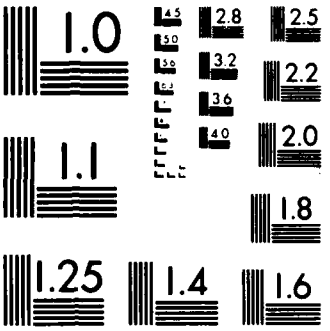

NAVAL POSTGRADUATE SCHOOL
Monterey, California

THESIS

UNSTEADY FLOW ABOUT
CAMBERED PLATES

by

Paul Daniel Munz

June 1987

Thesis Advisor T. Sarpkaya

UNCLASSIFIED

SECURITY CLASSIFICATION OF THIS PAGE

REPORT DOCUMENTATION PAGE

1a REPORT SECURITY CLASSIFICATION UNCLASSIFIED	1b RESTRICTIVE MARKINGS
2a SECURITY CLASSIFICATION AUTHORITY	3 DISTRIBUTION/AVAILABILITY OF REPORT Approved for public release; distribution is unlimited
2b DECLASSIFICATION/DOWNGRADING SCHEDULE	
4 PERFORMING ORGANIZATION REPORT NUMBER(S)	5 MONITORING ORGANIZATION REPORT NUMBER(S)
6a NAME OF PERFORMING ORGANIZATION Naval Postgraduate School 6b OFFICE SYMBOL (If applicable) 69	7a NAME OF MONITORING ORGANIZATION Naval Postgraduate School
6c ADDRESS (City, State, and ZIP Code) Monterey, California 93943-5000	7b ADDRESS (City, State, and ZIP Code) Monterey, California 93943-5000
8a NAME OF FUNDING/SPONSORING ORGANIZATION 8b OFFICE SYMBOL (If applicable)	9 PROCUREMENT INSTRUMENT IDENTIFICATION NUMBER
8c ADDRESS (City, State, and ZIP Code)	10 SOURCE OF FUNDING NUMBERS PROGRAM ELEMENT NO / PROJECT NO / TASK NO / WORK UNIT ACCESSION NO

11 TITLE (Include Security Classification)
UNSTEADY FLOW ABOUT CAMBERED PLATES

12 PERSONAL AUTHOR(S) MUNZ, PAUL DANIEL

13a TYPE OF REPORT	13b TIME COVERED	14 DATE OF REPORT (Year, Month, Day)	15 PAGE COUNT
Mechanical Engineer	FROM _____ TO _____	1987 June	51

16 SUPPLEMENTARY NOTATION

17 COSATI CODES			18 SUBJECT TERMS (Continue on reverse if necessary and identify by block number)
FIELD	GROUP	SUB-GROUP	Unsteady Flow, Discrete Vortex Analysis, Parachute, Vortex Motion

19 ABSTRACT (Continue on reverse if necessary and identify by block number)

The evolution of a two dimensional, incompressible, rapidly decelerating, time-dependent viscous flow about a sharp-edged camber is simulated through the use of the discrete vortex model. Vorticity is represented by a distribution of discrete point vortices. Each vortex is convected in the velocity field, calculated locally using the Biot-Savart law. The roll-up of the vortex sheets, the distribution of velocity and pressure on the camber, and the drag force are calculated at suitable time intervals for a prescribed time-dependent flow. Experiments are carried out in a vertical water tunnel partly to measure the drag force and partly to record on a video tape the evolution of the wake. The measured and calculated characteristics of the flow, such as the growth of the wake and the forces acting on the camber are found to be in

20 DISTRIBUTION/AVAILABILITY OF ABSTRACT ☒ UNCLASSIFIED/UNLIMITED ☐ SAME AS RPT ☐ DTIC USERS	21 ABSTRACT SECURITY CLASSIFICATION UNCLASSIFIED
22a NAME OF RESPONSIBLE INDIVIDUAL Professor T. SARPKAYA	22b TELEPHONE (Include Area Code) (408) 646-3425 22c OFFICE SYMBOL 69Si

DD FORM 1473, 84 MAR 83 APR edition may be used until exhausted
All other editions are obsolete

SECURITY CLASSIFICATION OF THIS PAGE
UNCLASSIFIED

19. ABSTRACT (Continued)

good agreement. Furthermore, the numerical simulation provided a plausible explanation for the cause of parachute collapse, a phenomenon which gave impetus to the numerical and physical experiments described herein. The numerical model developed during the course of the investigation is applicable to any time-dependent flow about two-dimensional cambered plates (circular arcs).

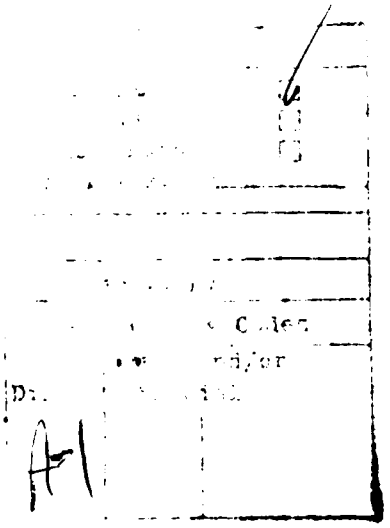

Approved for public release; distribution is unlimited.

Unsteady Flow About
Cambered Plates

by

Paul Daniel Munz
Lieutenant Commander, United States Navy
B.M.E., Villanova University, 1977

Subnitted in partial fulfillment of the
requirements for the degrees of

MASTER OF SCIENCE IN MECHANICAL ENGINEERING
and
MECHANICAL ENGINEER

from the

NAVAL POSTGRADUATE SCHOOL
June 1987

Author: Paul Daniel Munz
Paul Daniel Munz

Approved by:
T. Sarpkaya, Thesis Advisor

Anthony J. Healy, Chairman,
Department of Mechanical Engineering

G. E. Schacher,
Dean of Science and Engineering

ABSTRACT

The evolution of a two dimensional, incompressible, rapidly decelerating, time-dependent viscous flow about a sharp-edged camber is simulated through the use of the discrete vortex model. Vorticity is represented by a distribution of discrete point vortices. Each vortex is convected in the velocity field, calculated locally using the Biot-Savart law. The roll-up of the vortex sheets, the distribution of velocity and pressure on the camber, and the drag force are calculated at suitable time intervals for a prescribed time-dependent flow. Experiments are carried out in a vertical water tunnel partly to measure the drag force and partly to record on a video tape the evolution of the wake. The measured and calculated characteristics of the flow, such as the growth of the wake and the forces acting on the camber are found to be in good agreement. Furthermore, the numerical simulation provided a plausible explanation for the cause of parachute collapse, a phenomenon which gave impetus to the numerical and physical experiments described herein. The numerical model developed during the course of the investigation is applicable to any time-dependent flow about two-dimensional cambered plates (circular arcs).

TABLE OF CONTENTS

LIST OF TABLES

LIST OF FIGURES

TABLE OF SYMBOLS AND ABBREVIATIONS

4b	Chord Length of the Cambered Plate.
C_d	Drag Coefficient.
	$= D/2\rho b U_o^2$
C_l	Lift Coefficient.
	$= L/2\rho b U_o^2$
C_p	Pressure Coefficient.
c	Radius of the Circular Cylinder.
D	Drag Force (in Pounds/ft).
i	$= \sqrt{-1}$
q	Velocity Vector.
$\mathcal{R}$ [ ]	Real Part of a Complex Quantity.
Re	Reynolds Number.
r	Radial Distance.
T*	Nondimensional Time.
	$= Ut/c$
t	Time (in seconds).
U	Ambient Flow Velocity (in ft/s).
U_o	Reference Velocity.
U_s	Flow Velocity at Separation Point.
$\dot{U}$	Ambient Flow Acceleration (in ft/s^2)
u	x-Component of Velocity.
V_1	Tip Velocity.
V_2	Velocity at the Inner Edge of the Shear Layer.
V_t	Tangential Velocity Component.
v	y-Component of Velocity.
W	Complex Potential Function.
z	Nondimensional Location in the Physical Plane.
	$= x + iy$
z_n	Location of the n^{th} Vortex.
z_t	Tip Coordinate in the Physical Plane.
Δt	Time Increment.

Γ_n	Circulation of the n^{th} Vortex.
2α	Camber Angle.
ε	Radial Incremental Location of the Nascent Vortex.
ζ	Nondimensional Location in the Circle Plane. $= \xi + i\eta$
ζ_t	Coordinate of the Edge of the Camber in the Circle Plane.
ζ_0	Location of the Nascent Vortex in the Circle Plane.
θ	Angular Coordinate Measured Counter-Clockwise.
θ_s	Angular position of the Separation Point.
ν	Kinematic Viscosity (in ft^2/s).
ρ	Density (in $slugs/ft^3$).

ACKNOWLEDGEMENTS

It is with great respect and admiration that the author wishes to express his sincere thanks to Distinguished Professor T. Sarpkaya, for his enthusiastic help, guidance and advice throughout the course of this research. It has been a singular honor to work closely with such a dedicated professional. His zeal in the pursuit of knowledge has been inspiring and his friendship will be cherished.

The author also wishes to extend warm thanks to Colonel Samir I. M. Mostafa, Egyptian Air Force, for his invaluable help and advice during all aspects of this research, especially during the development of the computer program described herein.

The success of laboratory experiments conducted in conjunction with this investigation were in large measure due to the skill and craftsmanship of Mr. Jack McKay of the mechanical engineering department.

Lastly, the author wishes to acknowledge the contribution made by his wife Elizabeth. Without her love, support and understanding, this effort would not have been possible.

I. INTRODUCTION

A. SEPARATED FLOWS

The separated flow about bluff bodies has been almost completely unyielding to both analysis and numerical simulation for a number of mathematical reasons and fundamental fluid dynamic phenomena. Separation gives rise to the formation of free shear layers which roll up into vortex rings or counter-rotating vortices. They, in turn, interact with each other, with the counter-sign vorticity generated at the base of the body, and with the motion of often unknown separation points. The wake becomes unsteady even for a steady ambient flow and the problem of the determination of the characteristics of the wake becomes coupled to the conditions prevailing upstream of the separation points. Evidently, viscosity modifies radically the inviscid flow, which, in this case, cannot serve even as a first approximation to the actual flow. The boundary layer equations are not applicable beyond the separation points and are, therefore, of limited use in bluff-body flow problems.

The separated unsteady flow situations involving wake return, as in the case of a decelerating or oscillating body, are an order of magnitude more complex than those where the vortices continuously move away from the body. The net effect of the wake return is twofold. Firstly, the proximity of the large vortices dramatically affects the boundary layer, outer flow, pressure distribution, and the generation and survival rate of the new vorticity. Secondly, the vortices not only give rise to additional separation points and or additional vortices, but also strongly affect the motion of the primary vortices. These effects are further compounded by the diffusion and decay of vortices and by the three-dimensional nature of the flow.

The existing finite difference and finite element methods cannot yet treat the high Reynolds number flows with sufficient accuracy for a number of reasons. The finite difference schemes require a very fine grid, a turbulence model, and a very large computer memory. It seems that the modelling of the turbulent stresses in the wake, particularly in time-dependent flows will be the major source of difficulty in all future calculations. Whether or not it will ever be practical to apply the finite difference and finite element methods to high Reynolds number flows is unknown. The inherent difficulties are certainly significant enough to warrant exploring other solution methods.

Certain separated time-dependent flows may be simulated through the use of the discrete vortex model (DVM) (see e.g., Chorin 1973; Sarpkaya 1975). The free shear layers which emanate from the sides of the body are represented by an assembly of discrete vortices. The strength of the elemental vortices are determined through the use of the Kutta condition. The use of a suitable convection scheme enables one to march in time and to calculate the evolution of the wake, the velocity and pressure distributions, and the lift and drag forces acting on the body. The work described herein deals with the application of the DVM to decelerating flow about a two-dimensional camber.

B. FLOW ABOUT A CAMBERED PLATE AND PARACHUTE COLLAPSE

The determination of the deployment sequence of an axisymmetric porous parachute and the unsteady aerodynamic loads acting on it present a very complex coupled problem. The development of an analytical or numerical model which takes into account the effects of porosity, gaps, and variable opening schemes would allow numerical experiments on a large class of parachutes, reduce the number of expensive field tests to a few judiciously selected ones, and enable the designer to calculate the time history of the fall of the parachute and the strength required to survive the aerodynamic loads. However, the development of such a model is hampered by a number of difficulties.

The previous models for parachute loads are based by and large on empirical assumptions (see e.g., Heinrich and Saari 1987; Mcwey 1972). They rely on the observation that families of parachutes open in a characteristic length and seem to have aerodynamic properties that relate well to the projected area of the parachute. The apparent mass is assumed to be a function of the projected area only and is not a function of the prevailing flow characteristics. The vortex sheet analysis was used by Klimas (1977) to derive the acceleration-independent apparent mass coefficient for arbitrary-shaped axisymmetric surfaces. Muramoto and Garrard (1984) used a continuous-source model to predict the steady-state drag of ribbon parachutes. The analyses did not, however, deal with the evolution of the unsteady wake and its interaction with the canopy.

It is in view of the foregoing that a fundamental study of the separated time-dependent flow about two-dimensional rigid cambered plates was undertaken. Clearly, the flow about a rigid cambered plate is considerably simpler than that about a porous,

axisymmetric, and flexible parachute and the results, regardless of the degree of their agreement with corresponding experiments, may not have direct relevance to the practical problem under consideration. But the object of this investigation was the understanding of the evolution of the wake under controlled conditions rather than to provide a design tool. It is hoped that an investigation of this type will reveal the underlying physics of the phenomenon (particularly that of the parachute collapse), help to interpret the full-scale results and will provide inspiration for the development of more general vortex models with which the dynamics of axisymmetric, porous, and flexible parachute canopies can be investigated.

II. ANALYSIS

A. TRANSFORMATIONS AND THE COMPLEX VELOCITY POTENTIAL

The calculation of the velocity of any one of the vortices and the force acting on the body requires a conformal transformation (in which the camber becomes a circle), a complex-velocity potential representing the vortices, their images, and the two-dimensional irrotational flow around the body, and the use of the generalized Blasius theorem.

The flow in the circle plane may be transformed to that about a cambered plate through the use of two successive transformations, one from ζ plane to the ζ° plane and the other from the ζ° plane to the z plane. These are given by (see Fig. 2.1)

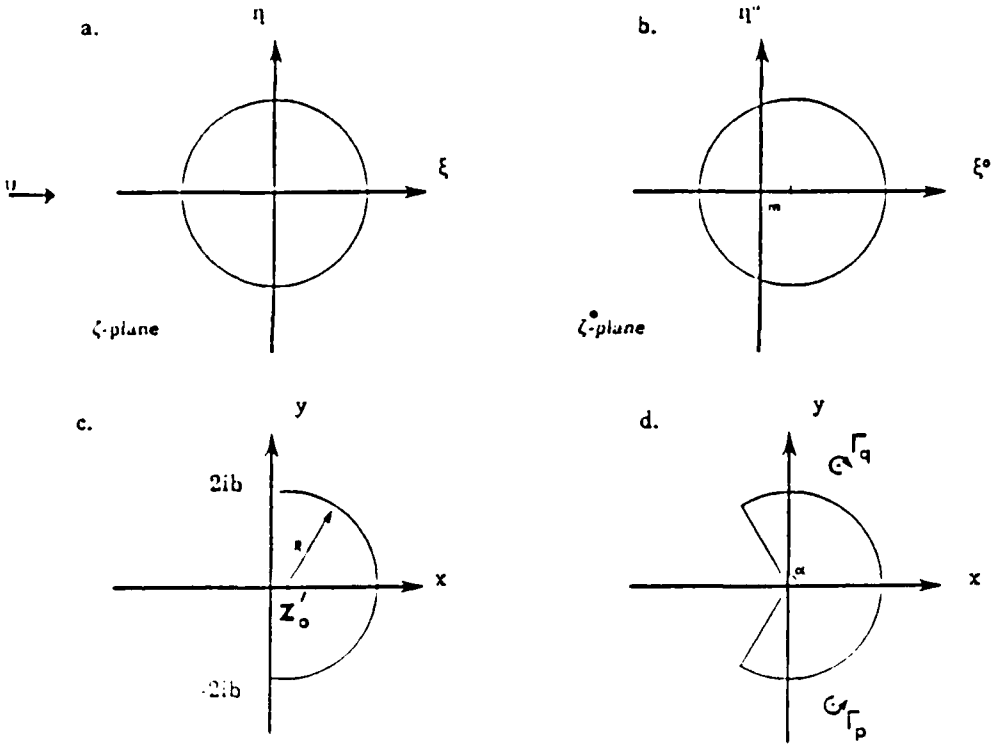

Figure 2.1 Circle and physical planes

$$z = \zeta^o - \frac{b^2}{\zeta^o}, \quad \text{and } \zeta^o = \zeta + m \tag{2.1}$$

Combining the two, one has a direct transformation from the ζ plane to the z plane as

$$z = \zeta + m - \frac{b^2}{\zeta + m} \tag{2.2}$$

It is easy to show that the camber in the z plane is a circular arc.

The y-axis in the z plane passes through the tips of the camber. It is advantageous to locate the origin of the coordinate axes at the geometric center of the camber. i.e., at the center of the circle part of which represents the camber. This is easily accomplished by shifting the origin of the coordinate axes by

$$z_o' = \frac{2m^2 - 1}{m} \tag{2.3}$$

where z_o' is the x coordinate of the origin of the circle in the z plane. Thus, one has

$$z = \zeta + m - \frac{b^2}{\zeta + m} + z_o, \quad \text{with } z_o' = -z_o \tag{2.4}$$

which transforms the circle in Fig. 2.1a to the physical plane in Fig. 2.1d. Table 1 summarizes the relationship between m, z_o', the included angle of the camber, b, and the radius of the camber.

TABLE 1

SUMMARY OF THE PARAMETRIC RELATIONSHIP

m	z_o'	2α	b	R = 1/m
cos60 = .5	-1	120	.866	2
cos45 = .707	0.	180	.707	$\sqrt{2}$
cos30 = .866	$1/\sqrt{3}$	240	.5	$2/\sqrt{3}$

The complex potential function W in the circle plane (see Fig. 2.1a) which describes a uniform flow U (assumed to be time-dependent) with a doublet at the origin to simulate the cylinder, Γ_{kq} clockwise-rotating vortices (called q-vortices), Γ_{kp} counter-clockwise rotating vortices (called p-vortices), and the images of all the p-and q-vortices in the circle plane may be written as

$$W = -U(\zeta + \frac{c^2}{\zeta}) + \frac{i\Gamma_{0p}}{2\pi} Ln(\zeta - \zeta_{0p}) - \frac{i\Gamma_{0p}}{2\pi} Ln(\zeta - \frac{c^2}{\overline{\zeta}_{0p}})$$

$$+ \sum_{k=1}^{m} \frac{i\Gamma_{kp}}{2\pi} Ln(\zeta - \zeta_{kp}) - \sum_{k=1}^{m} \frac{i\Gamma_{kp}}{2\pi} Ln(\zeta - \frac{c^2}{\overline{\zeta}_{kp}}) - \frac{i\Gamma_{0q}}{2\pi} Ln(\zeta - \zeta_{0q})$$

$$+ \frac{i\Gamma_{0q}}{2\pi} Ln(\zeta - \frac{c^2}{\overline{\zeta}_{0q}}) - \sum_{k=1}^{m} \frac{i\Gamma_{kq}}{2\pi} Ln(\zeta - \zeta_{kq}) + \sum_{k=1}^{m} \frac{i\Gamma_{kq}}{2\pi} Ln(\zeta - \frac{c^2}{\overline{\zeta}_{kq}}) \qquad (2.5)$$

in which Γ_{kp} and ζ_{kp} represent respectively the strength and location of the k-th p-vortex, Γ_{kq} and ζ_{kq} the strength and location of the k-th q-vortex, and c the radius of the cylinder; an overbar indicates a complex conjugate. The need for the separate identification of the p-and q-vortices and for the singling out of one of the vortices in each shear layer (namely Γ_{0p} and Γ_{0q} i.e., the nascent vortices) will become apparent later.

B. COMPLEX VELOCITIES OF VORTICES

The convection of the vortices and the calculation of the forces acting on the body require the evaluation of the velocities at the vortex centers. For the velocities in the circle plane this reduces to subtracting from Eq. (2.5) the complex potential corresponding to the vortex for which the velocity components are to be determined and evaluating the derivative of the remaining terms at $\zeta = \zeta_k$. To determine the velocities in the physical plane, however, one has to subtract $(i\Gamma_k/2\pi)\ Ln(z - z_k)$ from Eq. (2.5) or, in terms of ζ , the terms (see e.g., Sarpkaya 1967, 1975)

$$\frac{i\Gamma_k}{2\pi} Ln\,(\zeta - \zeta_k) + \frac{i\Gamma_k}{2\pi} Ln\,(1 - \frac{c^2}{\zeta\zeta_k}) \qquad (2.6)$$

It should be noted that the first term in Eq. (2.6) is the complex function corresponding to the k-th vortex in the ζ plane. The second term appears merely as a consequence of the transformation used. It is easy to show that for a p-vortex Eq. (2.6) may be reduced to (see e.g., Mostafa 1987)

$$-\frac{i\Gamma_{kp}}{2\pi}\frac{(-b^2)(\zeta_{kp}+m)}{[(\zeta_{kp}+m)^2+b^2]^2} \tag{2.7}$$

A similar expression can be written for the q-vortex.

C. KUTTA CONDITION

The fact that the flow separates tangentially with a finite velocity at the edges of the plate (Kutta condition) may be expressed by requiring

$$\frac{dW}{d\zeta} = 0 \qquad \text{at } \zeta = \zeta_t = -m \pm ib \tag{2.8}$$

Thus, inserting Eq. (2.5) in Eq. (2.8) one has

$$+\frac{i\Gamma_{0p}}{2\pi}\frac{1}{\zeta_t-\zeta_{0p}}-\frac{1}{\zeta_t-\frac{c^2}{\bar{\zeta}_{0p}}}-\frac{i\Gamma_{0q}}{2\pi}\frac{1}{\zeta_t-\zeta_{0q}}-\frac{1}{\zeta_t-\frac{c^2}{\bar{\zeta}_{0q}}}$$

$$+\sum_{k=1}^{m}\frac{i\Gamma_{kp}}{2\pi}\frac{1}{\zeta_t-\zeta_{kp}}-\frac{1}{\zeta_t-\frac{c^2}{\bar{\zeta}_{kp}}}-\sum_{k=1}^{m}\frac{i\Gamma_{kq}}{2\pi}\frac{1}{\zeta_t-\zeta_{kq}}-\frac{1}{\zeta_t-\frac{c^2}{\bar{\zeta}_{kq}}}$$

$$-U\left(1-\frac{c^2}{\zeta_t^2}\right)=0. \tag{2.9}$$

Equation (2.9) may be decomposed into two parts as

$$+\frac{i\Gamma_{0p}}{2\pi}\left(\frac{1}{\zeta_t-\zeta_{0p}}-\frac{1}{\zeta_t-\frac{c^2}{\bar{\zeta}_{0p}}}\right)-\frac{i\Gamma_{0q}}{2\pi}\left(\frac{1}{\zeta_t-\zeta_{0q}}-\frac{1}{\zeta_t-\frac{c^2}{\bar{\zeta}_{0q}}}\right)$$

$$+(-u_o+iv_o)=0. \qquad (2.10)$$

where the terms containing the strength of the nascent vortices represent the velocity induced at the tip of the camber by the nascent vortices and the term in parenthesis the velocity at the tip due to all other vortices (and their images), the doublet at the center of the circle in the ζ plane and the ambient velocity.

Equation (2.10) represents two coupled equations for the strengths and positions of the nascent vortices. Thus, the solution of the said quantities does, in general, require an iteration. However, this iteration may be avoided by noting that the velocity induced by a nascent vortex at the opposite tip is very small and certainly negligible. Thus, Eq. (2.10) for one of the nascent vortices may be reduced to

$$-\frac{i\Gamma_{0q}}{2\pi}\left(\frac{1}{\zeta_t-\zeta_{0q}}-\frac{1}{\zeta_t-\frac{c^2}{\bar{\zeta}_{0q}}}\right)+(-u_o+iv_o)=0 \qquad (2.11)$$

A similar expression may be written for the other nascent vortex. The use of the Kutta condition, as expressed by Eq. (2.11), will be further explained following the discussion of the tip velocity. It suffices to note that all nascent vortices satisfying the Kutta condition do not yield either the same tip velocity or the same velocity distribution in the neighborhood of the tip. There are, in fact, certain preferred positions for the nascent vortices which yield physically realistic velocity distributions near the tips of the cambered plate. These nascent vortex positions have been determined by Mostafa (1987).

D. TIP VELOCITY

According to the Kutta condition the tangential velocity at the tip is finite. It may be determined through the use of l'Hopital's rule.

The velocity at the tip is given by

$$\frac{dW}{dz}=\frac{dW}{d\zeta}\frac{d\zeta}{dz} \qquad \text{at} \quad z_t=z_o\pm 2ib \qquad (2.12)$$

The use of l'Hopital's rule then yields,

$$\left.\frac{dW}{dz}\right|_{z=z_t} = \frac{d^2W}{d\zeta^2}\left(\frac{ib}{2}\right) \tag{2.13}$$

Equation (2.13) yields the desired finite tip velocities.

E. TIME DEPENDENT-FORCES

The force acting on the body in the physical plane may be calculated either through the use of the pressure distribution or through the use of the rate of change of impulse.

Bernoulli's equation for unsteady flow is given by

$$\left(\frac{P_1}{\rho} + \frac{V_1^2}{2}\right) - \left(\frac{P_2}{\rho} + \frac{V_2^2}{2}\right) - \int_1^2 \frac{\partial V}{\partial t}\,ds = f(t) \tag{2.14}$$

where the indices indicate two points on the body in the physical plane. Since there is no pressure drop across the shear layer and since the integral term in Eq. (2.14) is zero at the tip (i.e., ds = 0), one has

$$f(t) = \frac{V_{t1}^2}{2} - \frac{V_{t2}^2}{2} \tag{2.15}$$

where V_{t1} and V_{t2} represent the tangental velocities on the upstream and downstream faces of the tip. It is important to note that f (t) in Eq. (2.15) is also the time rate of change of circulation, i.e., the rate at which vorticity is shed into the wake from the tip of the cambered plate.

The normalized form of Bernoulli's equation between any two points m and n then becomes

$$\frac{P_m - P_n}{\rho U_o^2/2} = \frac{V_{t1}^2 - V_{t2}^2}{U_o^2} + \frac{V_n^2 - V_m^2}{U_o^2} + \frac{\partial}{\partial t}\int_m^n 2\,\frac{V}{U_o^2}\,ds \tag{2.16}$$

The integration of the differential pressure between the upstream and downstream faces of the camber yields the force components in the x and y directions, i.e., the drag and lift forces.

The force acting on the body can also be calculated through the rate of change of impulse. It is given by

$$F = 4\pi\rho c^2 \dot{U} \left(1 - \frac{m^2}{2c^2}\right) + \frac{\partial}{\partial t}\left[\Gamma_n (z_n - z_{ni})\right] \tag{2.17}$$

which may be written as

$$C_d + i C_l = \frac{F}{2\rho U_o^2 b} = 2\pi\left(\frac{c\dot{U}}{U_o^2}\right)\left(\frac{c}{b}\right)\left(1 - \frac{m^2}{2c^2}\right) + \frac{c}{2b}\frac{\partial}{\partial(U_o t/c)}\left\{\frac{\Gamma_k}{U_o c}\left[f\left(\frac{\zeta_k}{c}\right) - f\left(\frac{c}{\bar{\zeta}_k}\right)\right]\right\} \tag{2.18}$$

in which U_o is the reference velocity; $\dot{U}$, the rate of deceleration of flow and $z = f(\zeta_k)$, i.e., the transformation given by Eq. (2.4). Equation (2.18) may also be deduced directly from the generalized Blasius equation. It is important to note that the force calculated from Eq. (2.18) includes the effect of the rate of change of circulation between two successive time steps. Thus, it may be smaller or larger (depending on the sign of Γ) than the force calculated through the integration of the instantaneous differential pressure Eq. (2.16). This is because of the fact that the instantaneous pressure depends **only** on the prevailing flow conditions and does not account for the rate of change of total circulation between successive time steps. In the calculations to follow U_o and c are taken as unity for sake of simplicity.

F. METHOD OF CALCULATION

The methods used in the past in the determination of the vorticity flux from sharp-edged bodies may be roughly classified into two broad categories. The first of these involves the use of variable nascent vortex positions (see e.g., Sarpkaya 1968, 1975) and the second, the use of fixed nascent vortex positions (see e.g., Clements 1973-1975).

In the present analysis the method of variable nascent vortex positions is used. To explain the computational details of the method let us consider a particular time t after the start of the motion and assume t to be sufficiently large so that there are a number of vortices in the wake. Then the appearance and convection of the vortices proceed as follows:

(1) Select a vortex position along the radial line defined by $\theta = 117.72^{\circ}$ (see Mostafa 1987). The very first location is taken r = 1.1 .

(2) Calculate the strength of the nascent vortex which satisfies the Kutta condition. This is an exact solution and requires no iteration.

(3) Place the nascent vortex at the corresponding points in the circle and physical planes and calculate the tip velocity.

(4) Calculate a new nascent vortex strength from $0.5(V_1^2 - V_2^2)\Delta t$ where V_1 is the tip velocity and V_2, the average of three velocities along the radial line in the physical plane, i.e., at r = 1.05, 1.10 and 1.15.

(5) Compare the newly calculated circulation with that obtained from the Kutta condition. If the difference between the two circulations is less than 0.001 procede to the next step. If the said difference is larger than 0.001, carry out an iteration on the radial location of the nascent vortex as many times as necessary until the above condition is satisfied. If the circulation calculated from the Kutta condition is larger than that calculated from the tip velocities, the vortex must be moved towards the cylinder and vice versa. Also, each time the direction of the motion of the nascent vortex is changed (inward or outward), the marching distance is halved in order to accelerate the convergence of the two circulations.

(6) Calculate the velocity induced at the center of all other vortices;

(7) Convect the two nascent vortices with a velocity $0.5(V_1 + V_2)$ for a time interval Δt (note that the vorticity is convected with the average velocity of the shear layer).

(8) Convect all other vortices for the same time-interval Δt using a second order scheme given by

$$z(t+\Delta t) = z(t) + 0.5\,[3\dot{z}(t) - \dot{z}(t-\Delta t)\,]\,\Delta t \qquad (2.19)$$

in which $\dot{z} = u + iv$.

(9) Remove the vortices from the calculation whenever they come nearer than 0.05 to the camber in the physical plane (except the first 20 vortices from the tip);

(10) Coalesce the same sign vortices with a separation of less than 0.05 (in the physical plane, except the first 20 vortices);

(11) Calculate the tangential velocities and pressures on the inner and outer faces of the camber. Determine the drag and lift forces through the integration of pressure and through the use of the rate of change of impulse. Make plots of suitable variables (e.g., velocity distribution near the tip, variation of nascent vortex circulation with time, evolution of the wake, etc.);

(12) Check the flow conditions to determine the state of the calculations:

(a) If $V_1 - V_2 > 0.1$ repeat the foregoing steps;

(b) Stop the introduction of nascent vortices if $0 < V_1 - V_2 < 0.1$ and return to step No. 6;

(c) If $V_2 > V_1$ switch the angular positions of the nascent vortices to their image points. Calculate V_2 as the average of the three velocities, at the upstream side of the tip of the camber, at three radial locations (0.95, 0.9, and 0.85) and repeat the foregoing steps; and

(13) Make plots of the variations of various flow parameters (e.g., tip velocity, nascent vortex circulation, evolution of the wake, force coefficients, etc.) and terminate the run.

The foregoing steps are quite general and can be used for any camber, provided that the optimum points of placement of the nascent vortices are determined through the use of a method developed by Mostafa (1987).

III. DISCUSSION OF RESULTS

A. NUMERICAL AND PHYSICAL EXPERIMENTS

The calculations were carried out for a time-dependent normalized velocity given by

$$\frac{U}{U_o} = 1 \quad \text{for} \quad T = \frac{U_o\, t}{c} \leq 9.72 \tag{3.1}$$

and

$$\frac{U}{U_o} = 0.97T - 0.05T^2 - 3.70 \tag{3.2}$$

and

$$A = 0.97 - 0.10T \tag{3.3}$$

in the interval $9.72 \leq T \leq 11.48$ and

$$U = -0.3423T + 0.0072T^2 + 3.82 \tag{3.4}$$

and

$$A = -0.3423 + 0.01445T \tag{3.5}$$

in the interval $11.48 \leq T. \leq 17.95$. For T larger than 18, the velocity and acceleration are zero. These velocities and accelerations correspond to that encountered in a series of experiments carried out in a vertical water tunnel. A detailed description of the equipment and procedures is given by Sarpkaya and Ihrig (1986) and will not be repeated here. Evidently, the calculations can be carried out for any specified variation of the velocity. For the case under consideration, the flow begins to decelerate at T*

= 9.72 and the velocity of the ambient flow reduces to zero at about T* = 18. (see Fig. 3.1)

The computer program provided, at times specified, the positions of all the vortices, the rate of shedding of vorticity from the tips of the camber, the velocity distribution on the upstream and downstream faces of the camber, the differential pressure distribution, and the force coefficients.

Figures 3.2 through 3.5 show, at $T^* = U_o t/c = 6.00$, the evolution of the wake, the differential pressure distribution, and the velocities at the upstream and downstream faces of the camber. Figures 3.6 through 3.17 show similar plots of the wake, pressure, and velocity at larger times. These and other figures (not reproduced here for sake of brevity) show that the characteristics of the flow develop symmetrically prior to the onset of deceleration ($T^* < 9.72$) and the differential pressure is positive everywhere (i.e., the pressure inside the camber is larger than that outside).

Following the onset of deceleration (see e.g., Figs. 3.8, 3.12, and 3.16), the differential pressure near the axis of the camber becomes increasingly negative. The significance of this result is that had the model been flexible (as in the case of a parachute) the central part of the camber would have collapsed as a result of the particular deceleration it is subjected to.

For T* larger than about 13 (for the ambient flow under consideration), the velocities induced at the downstream edges of the camber by the large vortices moving sideways and towards the camber give rise to oppositely-signed vorticity. This, in turn, leads to the rapid growth of the secondary vortices (see e.g., Figs. 3.14 and 3.15 at T* = 21.275). Attention is drawn to the fact that the differential pressure shown in Fig. 3.16 is negative over a large central portion of the camber.

Figure 3.18 shows the variation of the circulation of the nascent vortex with T*. As expected, the vorticity flux is quite large at the start of the motion. It decreases gradually prior to the onset of deceleration and rapidly thereafter. For T* larger than about 12, i.e., when the secondary vortices come into existence, the circulation becomes negative. It reaches a minimum value when the ambient velocity and acceleration reduce to zero (at about T* = 18). The subsequent motion of the primary and secondary vortices increases the tip velocity and hence the strength of the nascent vortices. Nevertheless, the circulation remains negative, i.e., only the secondary vortices continue to receive additional vorticity.

Figure 3.19 shows the velocities V_1 and V_2 as a function of T*. The tip velocity V_1 decreases from an initially large value of about 3 to a nearly constant value of about 1.4 just prior to the onset of deceleration. Subsequently, V_1 decreases rapidly during the period of deceleration and prior to the inception of the secondary separation. Then V_1 increases to about 2 because of the backward motion of the large vortices near the tips of the camber. Finally, V_1 decreases once again as the primary and secondary vortices move sideways and away from the tips of the camber due to their mutual induction (see Fig. 3.15).

The variation of V_2 with T* is significant only during two, relatively short, time intervals: at the start of the motion and at the start of the deceleration. These are the periods during which the vorticity flux changes rapidly in order to maintain the Kutta condition. During the remainder of time V_2 is negligibly small, as expected on the basis of the pioneering experiments of Fage and Johansen (1928) with steady flow over various types of bluff bodies.

Figure 3.20 shows the variation of the drag coefficient as a function of T*. It is calculated through the the integration of pressure about the camber. Figure 3.20 also shows that C_d rises rapidly (due to the rapid accumulation of vorticity in the growing vortices) and begins to decrease as the vortices develop under the influence of a constant ambient velocity. Then the force decreases sharply at the onset of deceleration and goes through zero near the middle of the deceleration period (T* = 14). The force acquires its largest negative value towards the end of the deceleration period. Subsequently, the force gradually decreases to zero.

Figure 3.21 shows a comparison of the calculated and measured drag coefficients. In general the agreement between the calculated and the measured drag coefficient is quite good. The differences are primarily due to the fact that the diffusion of vorticity has not been taken into account in the numerical analysis. It is possible to introduce a small artificial reduction in circulation in order to bring the calculated and measured values into closer agreement. This has been avoided in the present analysis in order to keep the discrete vortex analysis as pure and simple as possible.

Finally, Fig. 3.22 shows a comparison of the normalized drag forces for various periods of the initial steady flow, prior to the onset of deceleration. It is clear that the drag forces beyond the point of deceleration are nearly identical. In other words, the force acting on the camber is not materially affected by the duration of the ambient steady flow within the range of the parameters encountered in the present study.

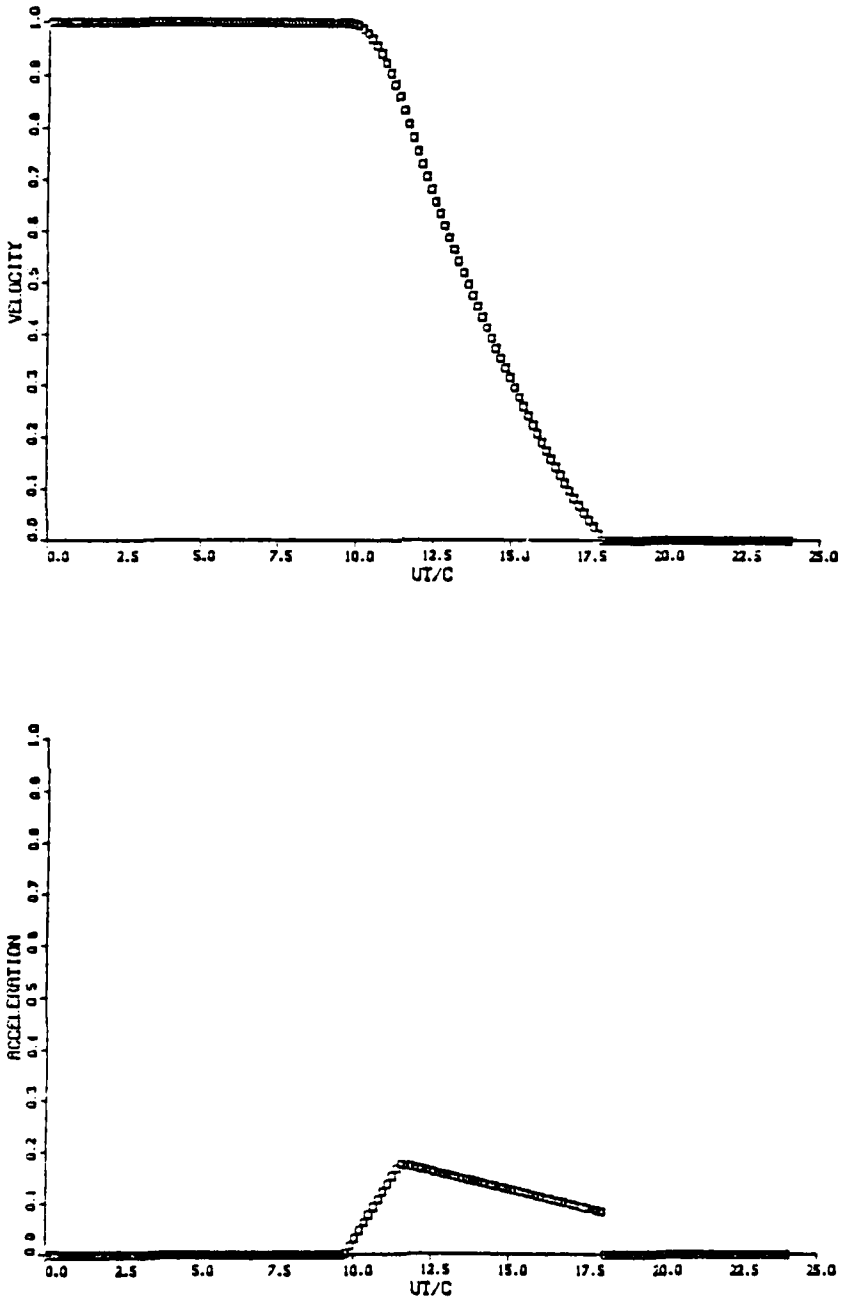

Figure 3.1 Variations of the velocity and acceleration with T*

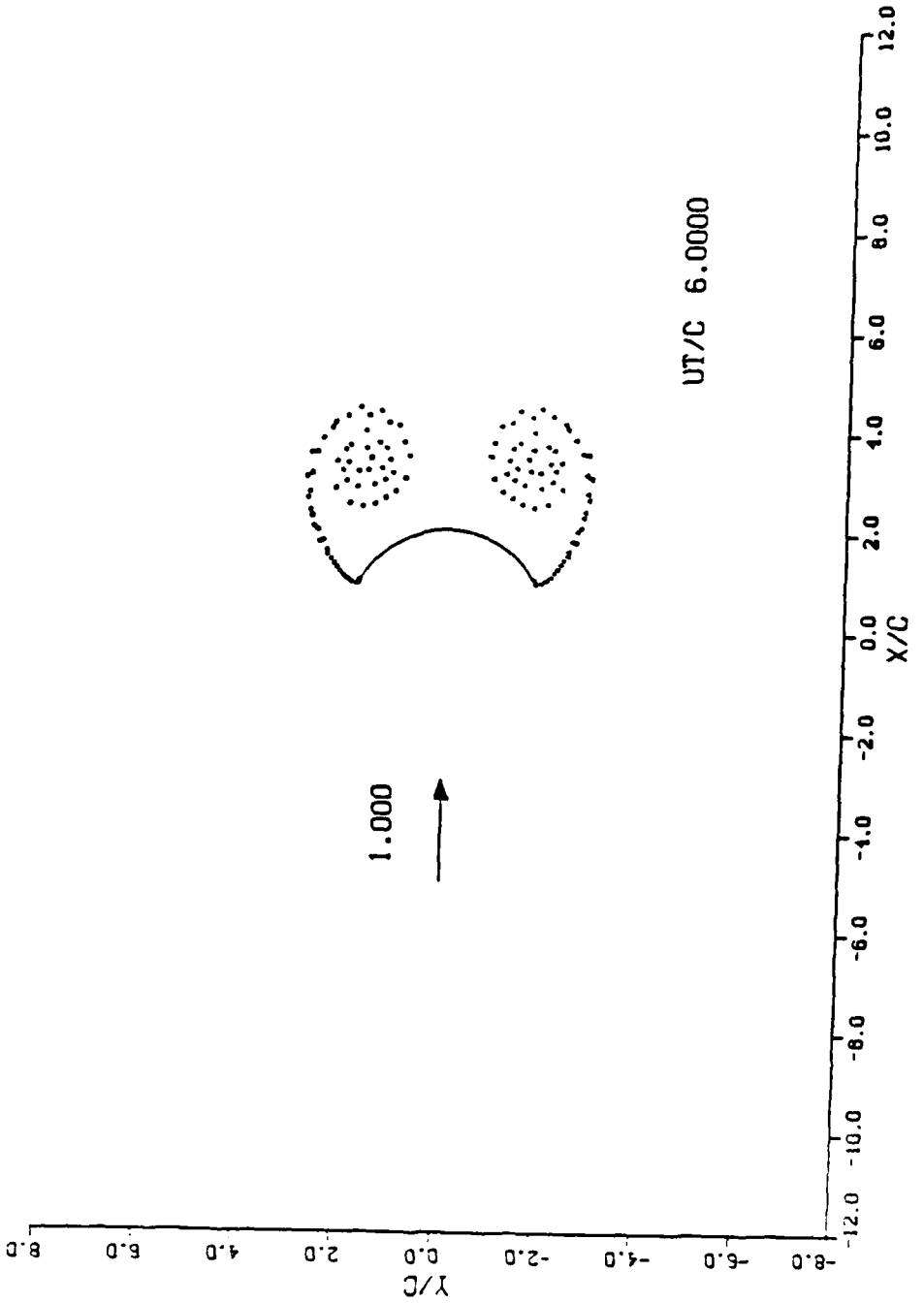

Figure 3.2 Position of vortices at $T^* = 6.00$

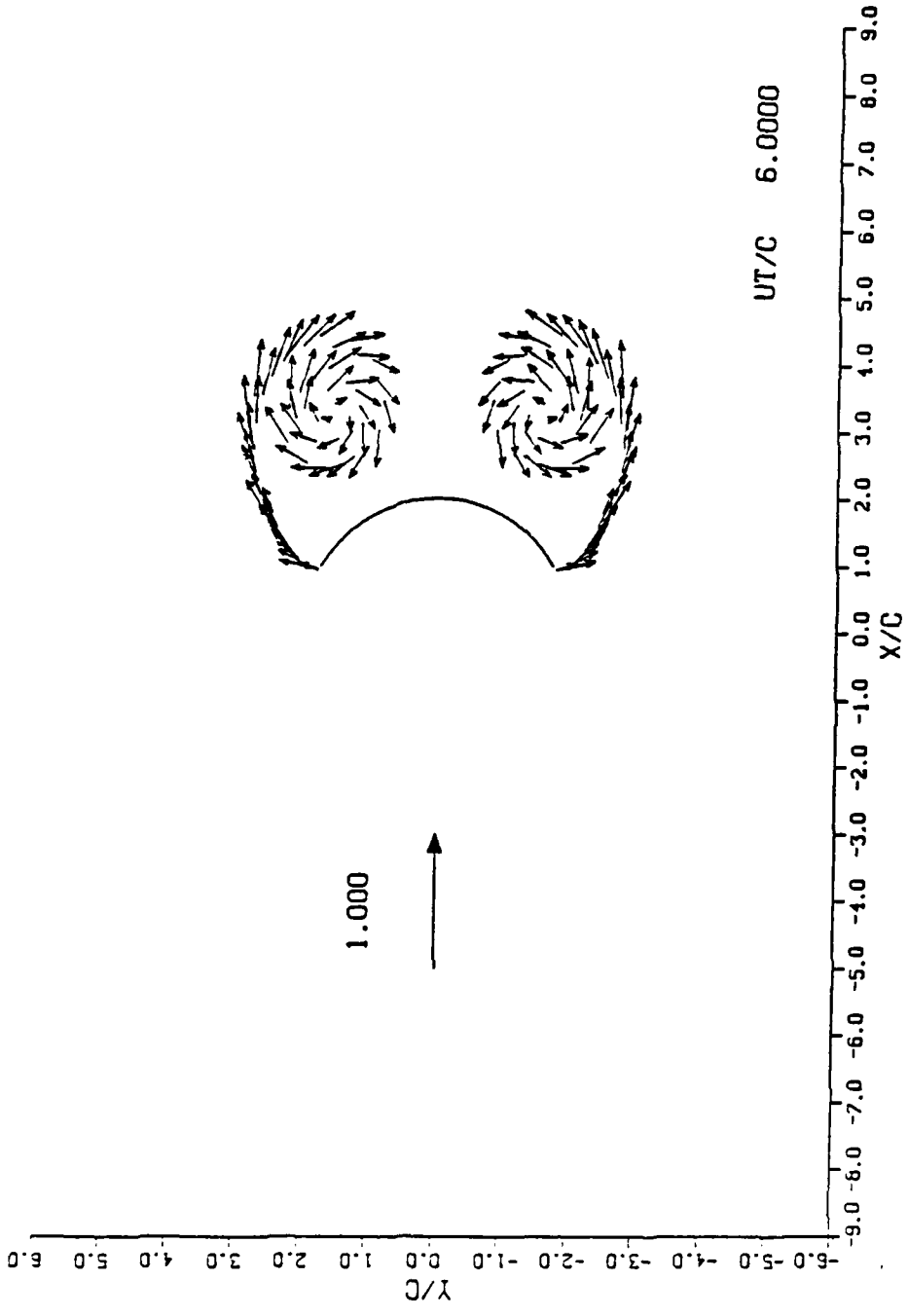

Figure 3.3 Instantaneous velocity of the vortices at T* = 6.00

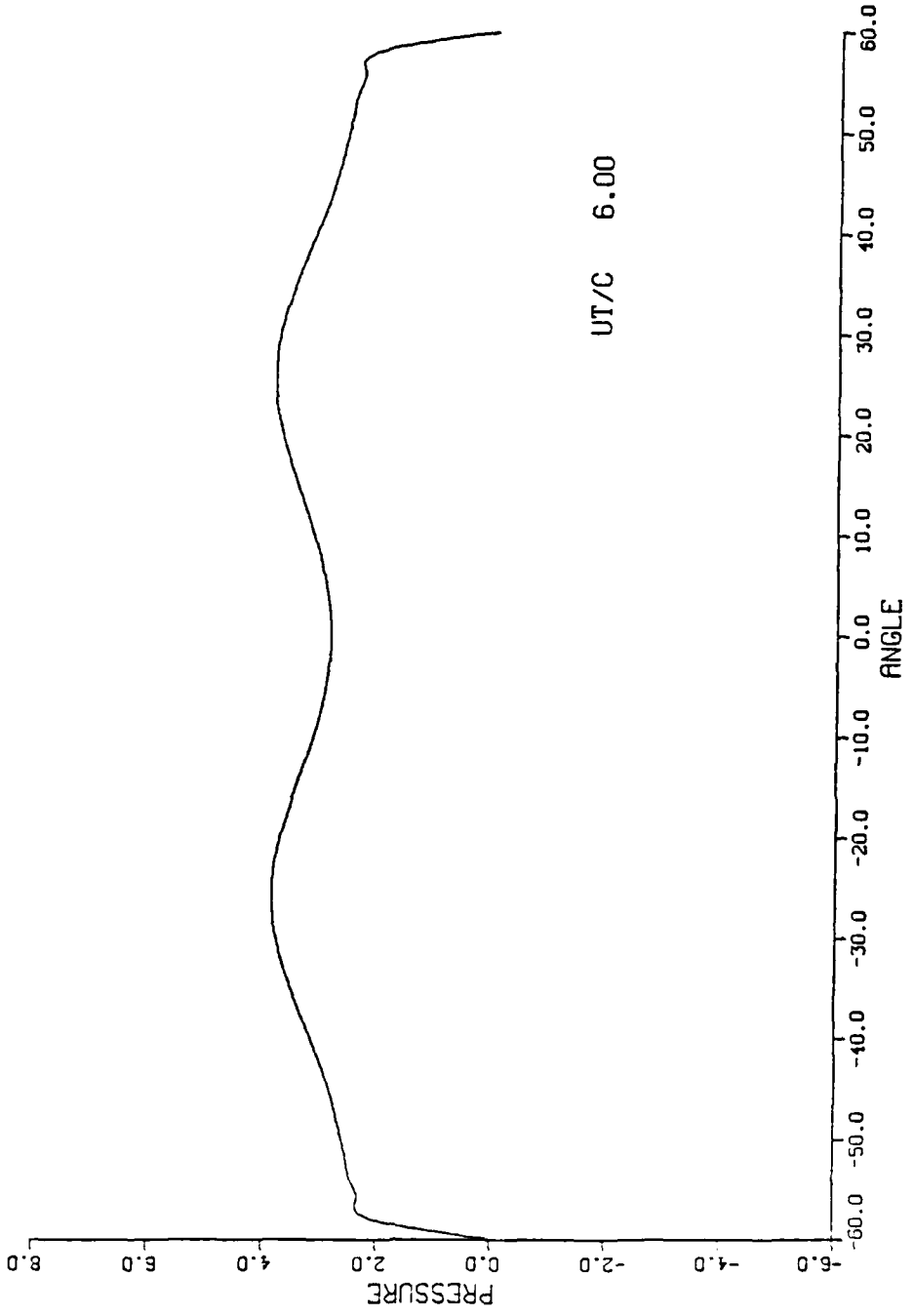

Figure 3.4 Differential pressure distribution at $T^* = 6.00$

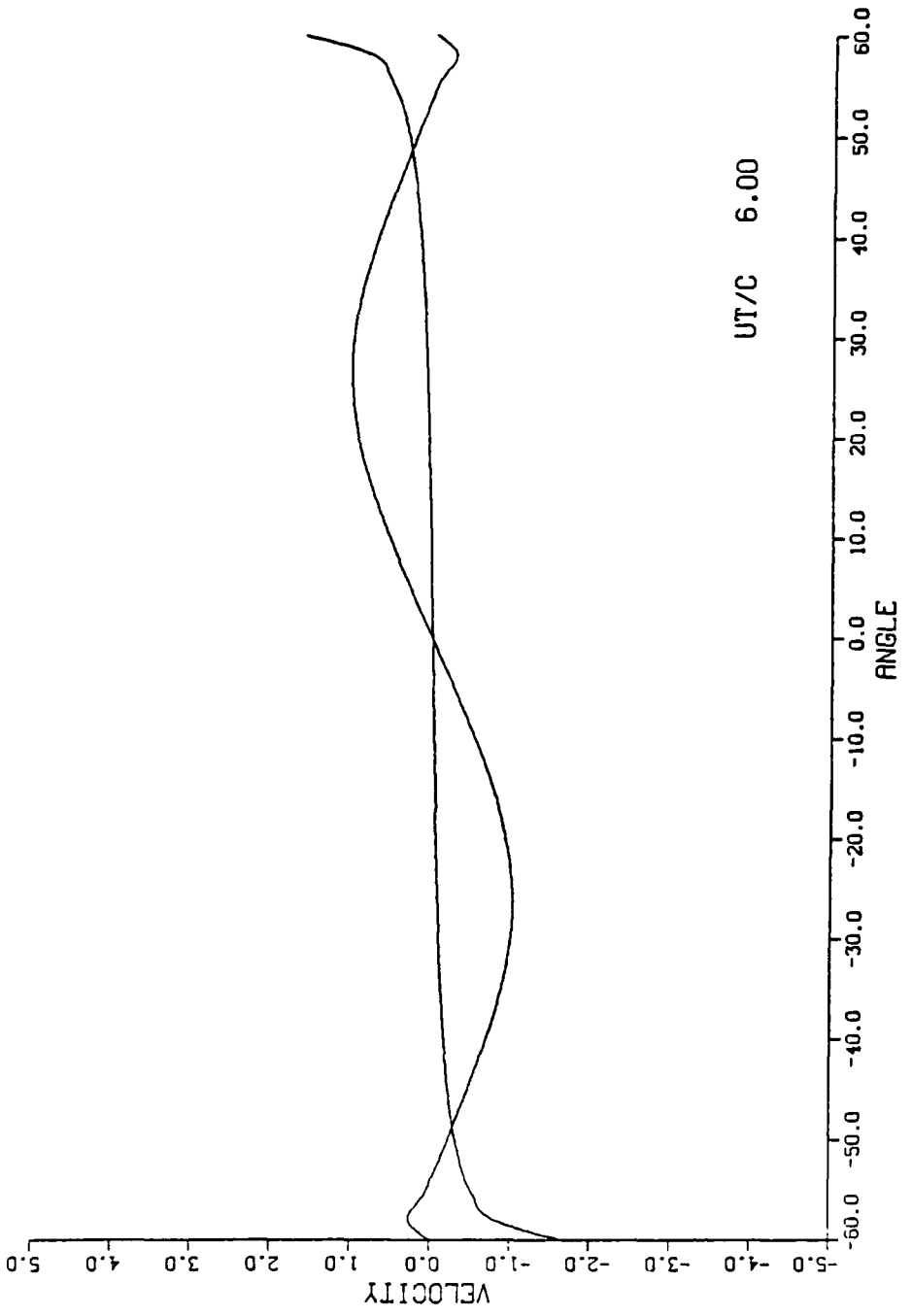

Figure 3.5 Velocity distribution on both faces of the camber at T* = 6.00

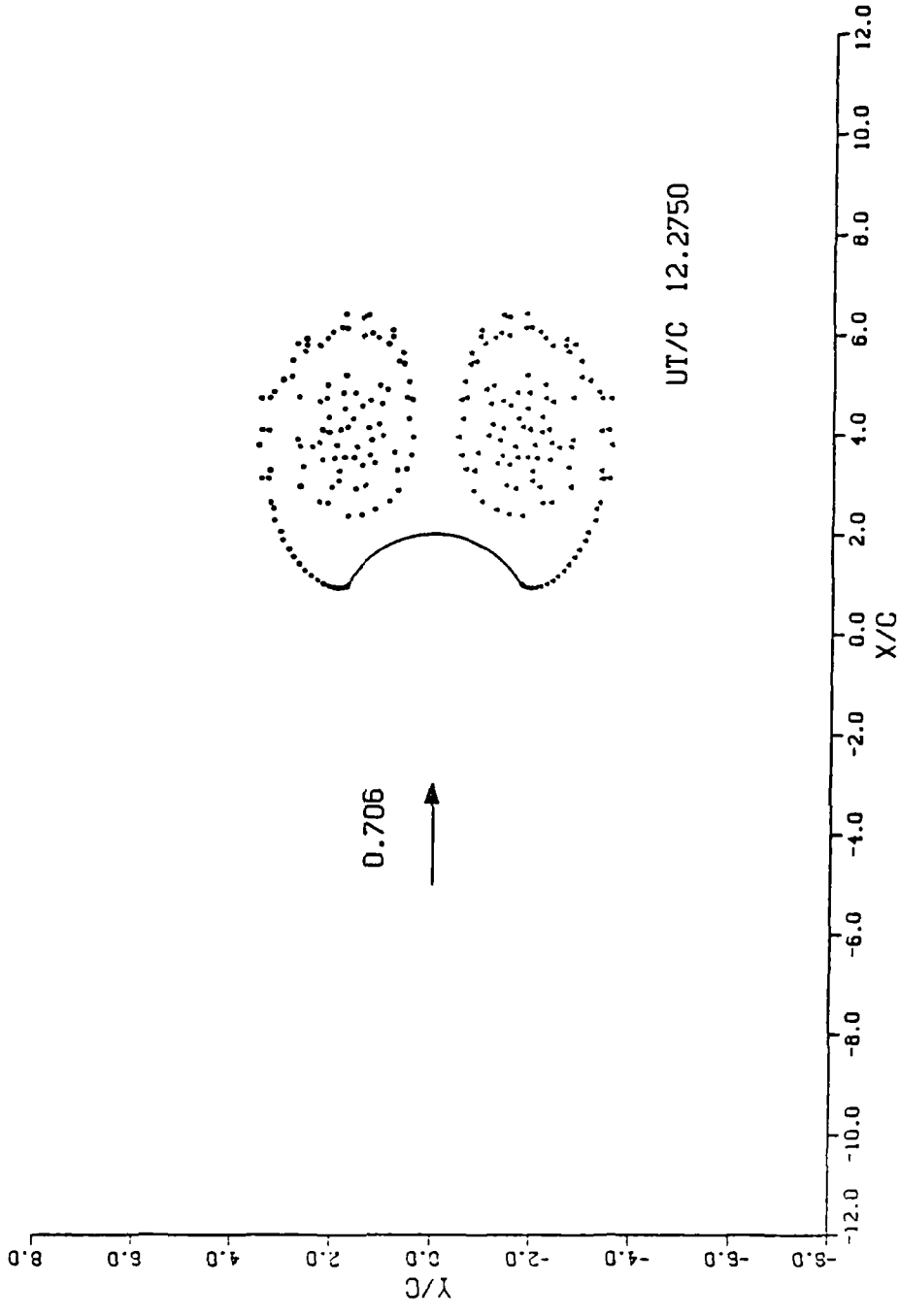

Figure 3.6 Position of vortices at $T^* = 12.275$

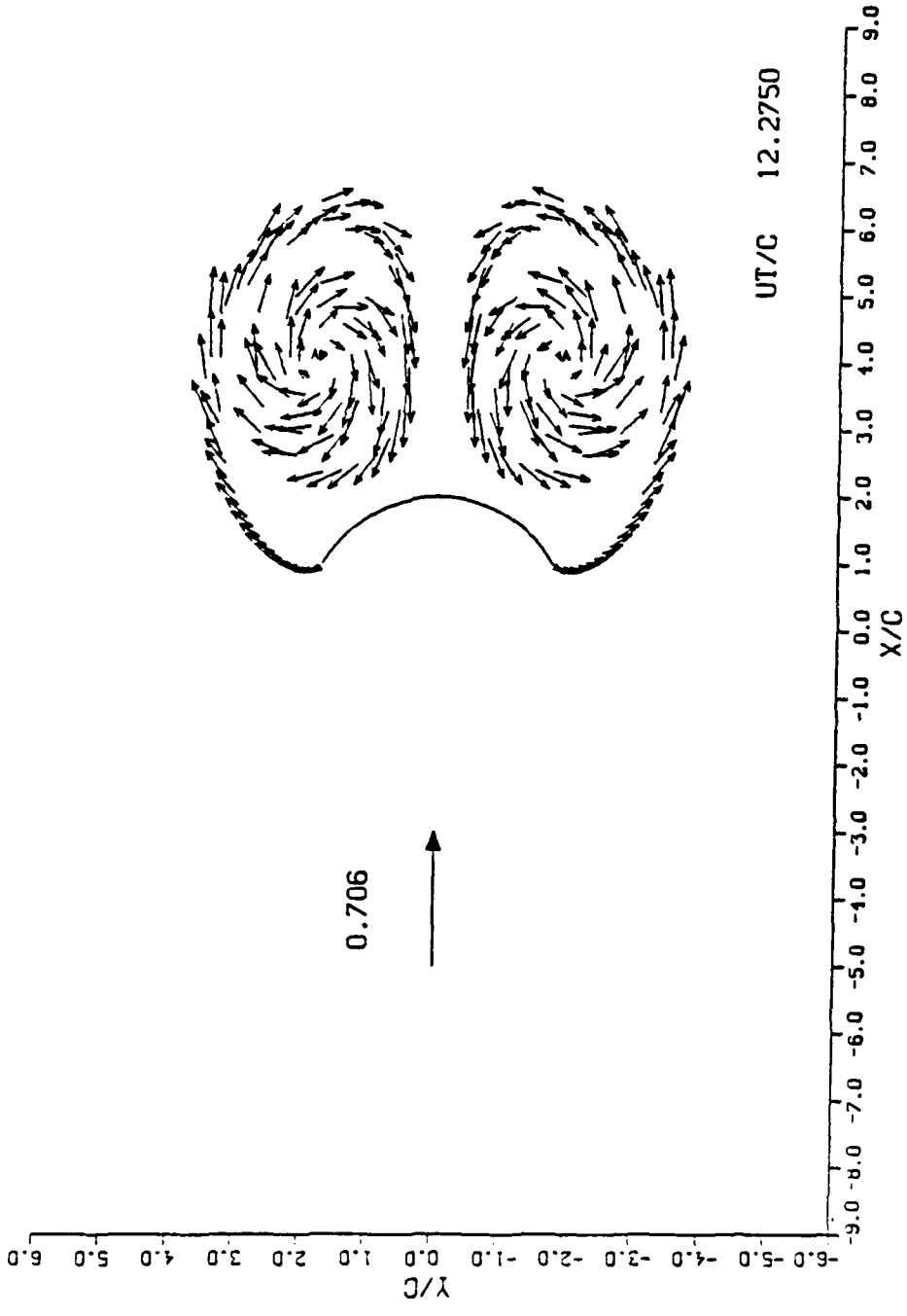

Figure 3.7 Instantaneous velocity of the vortices at $T^* = 12.275$

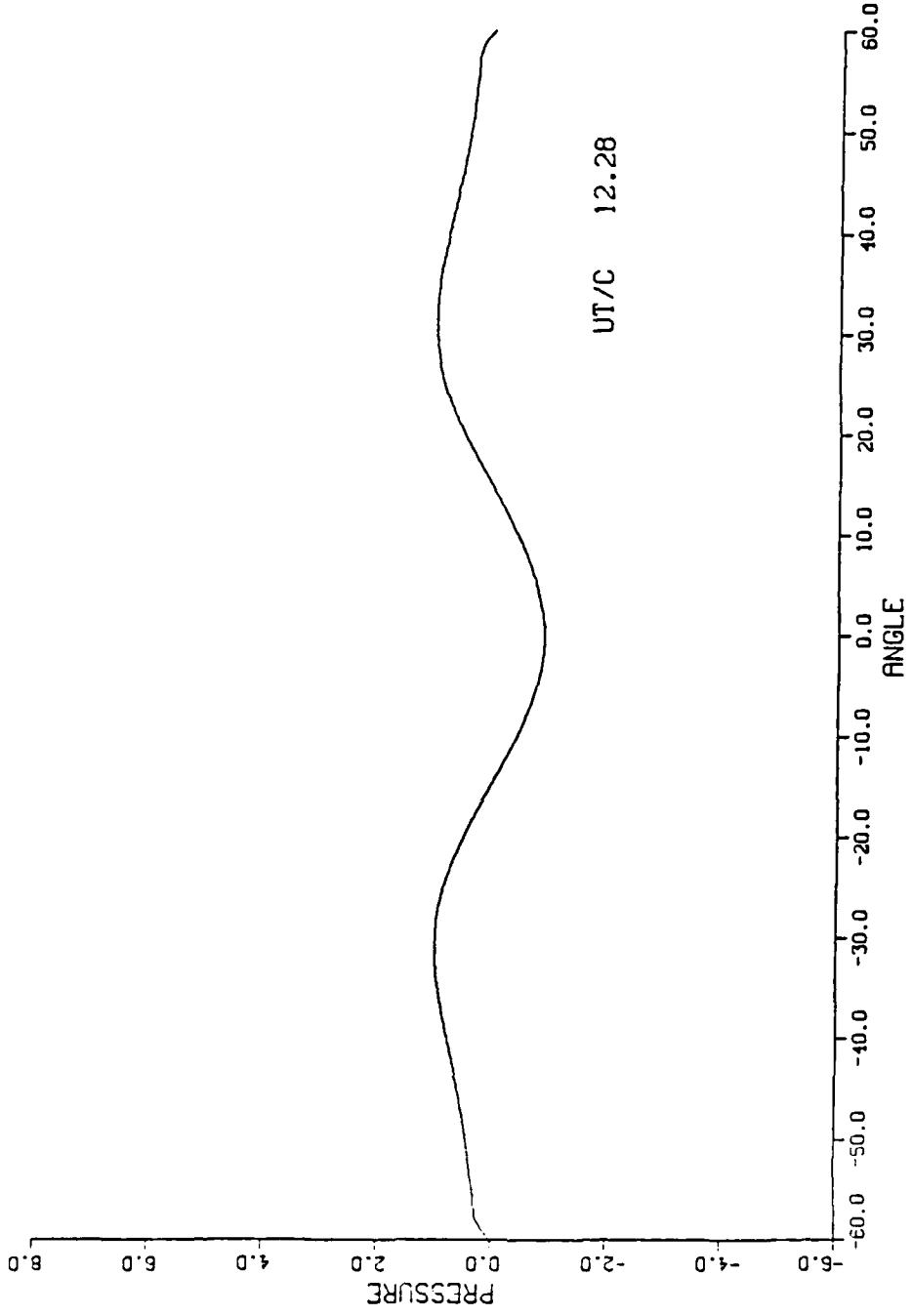

Figure 3.8 Differential pressure distribution at $T^* = 12.275$

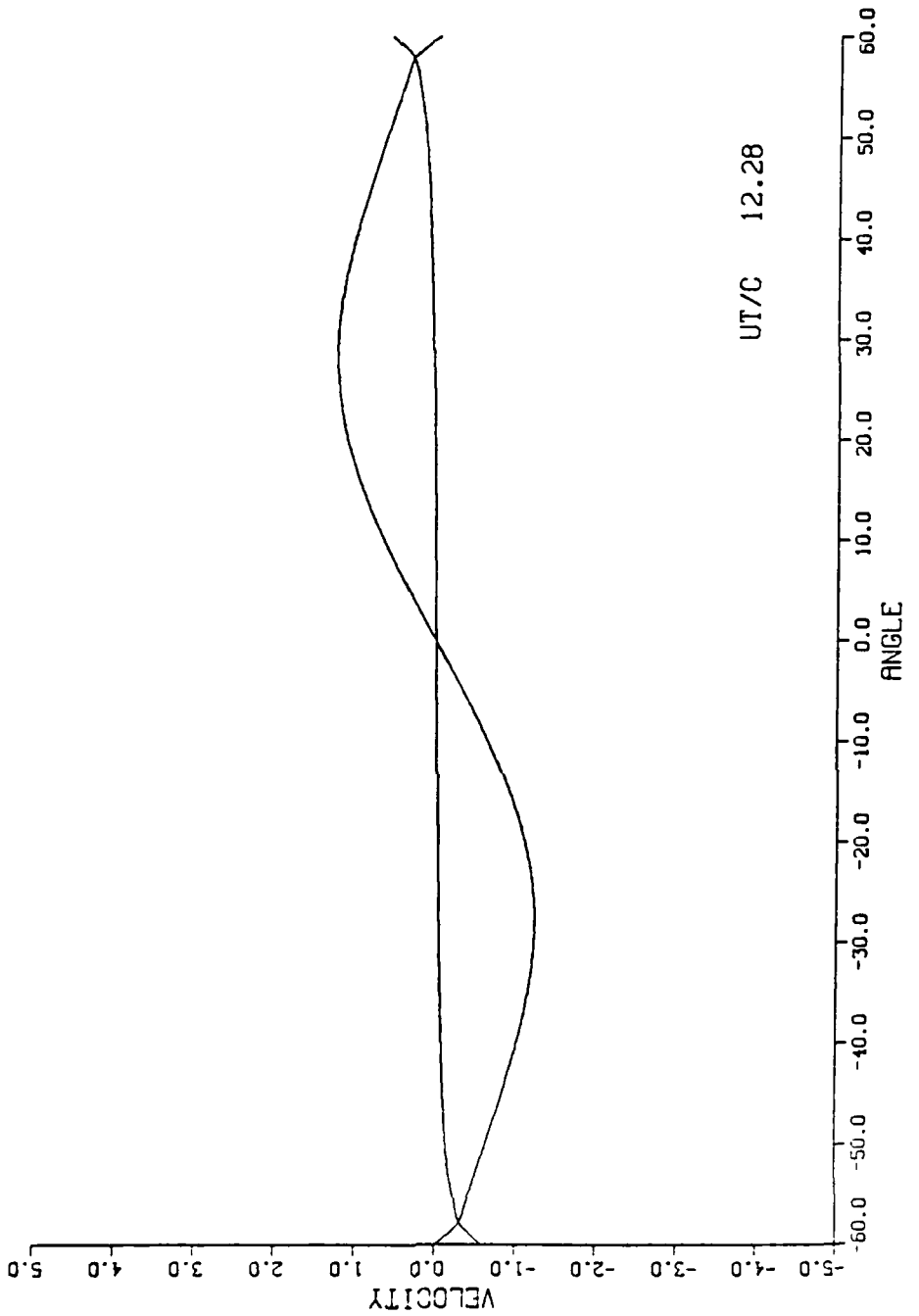

Figure 3.9 Velocity distribution on both faces of the camber at T* = 12.275

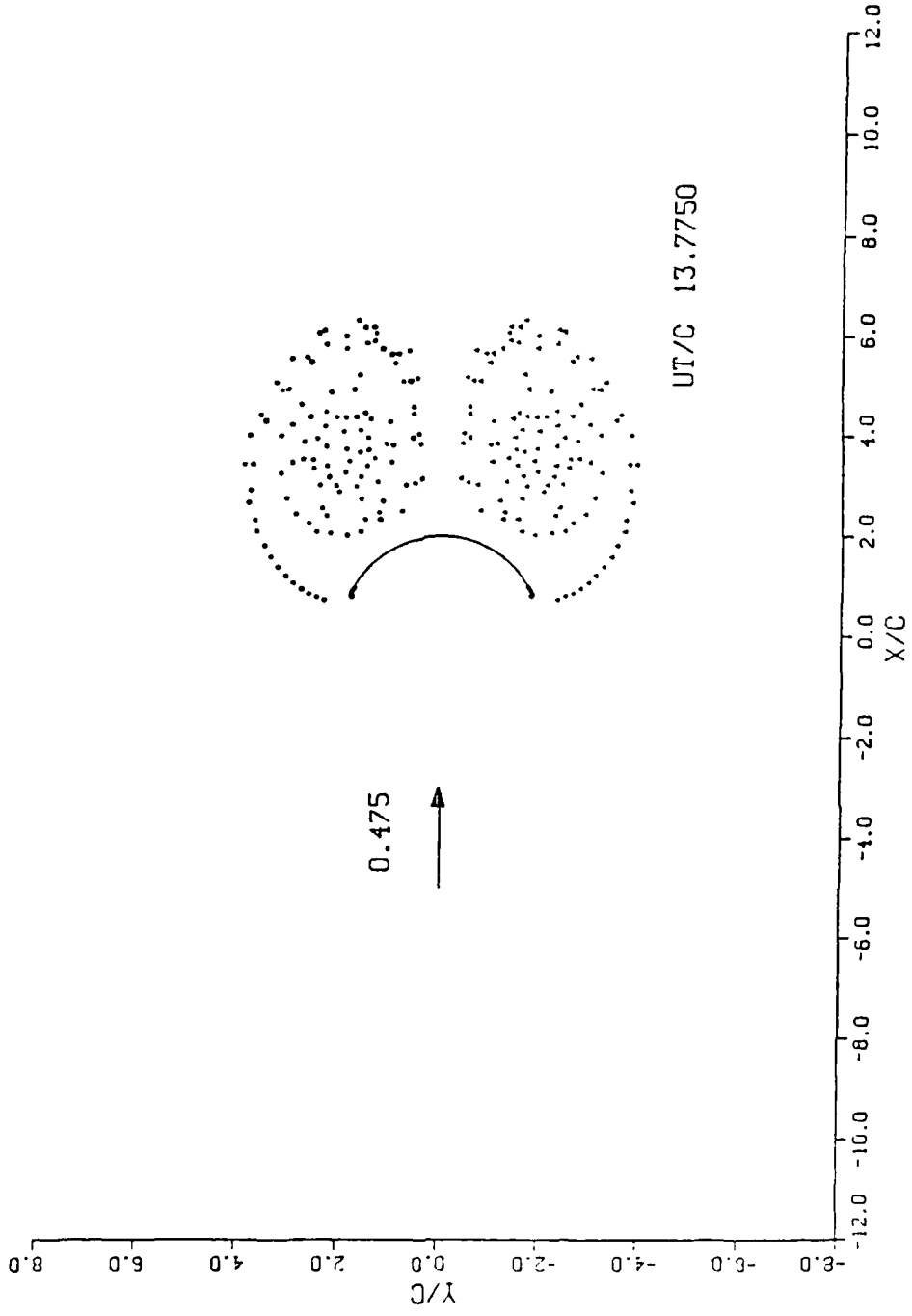

Figure 3.10 Position of vortices at T* = 13.775

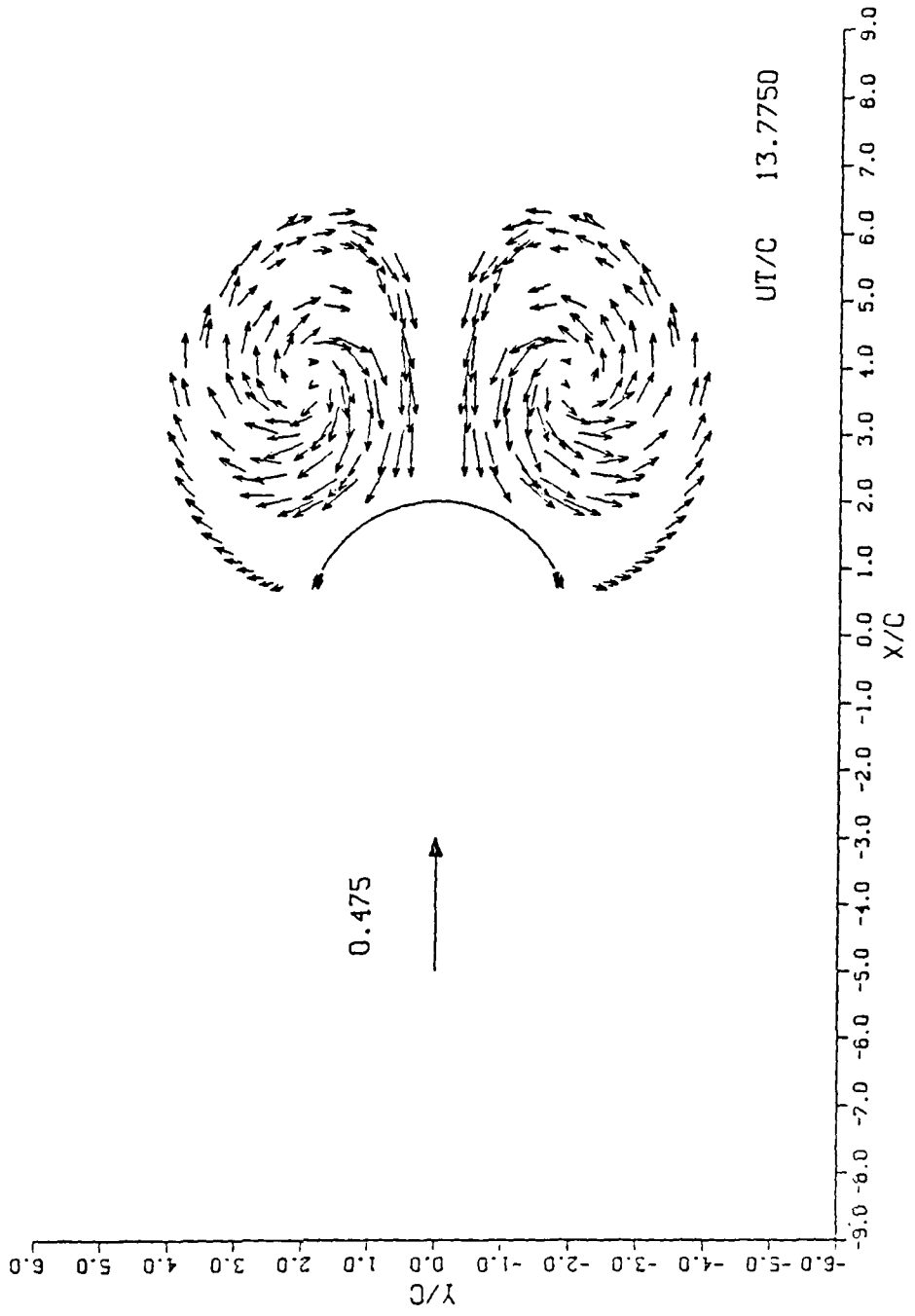

Figure 3.11 Instantaneous velocity of the vortices at T* = 13.775

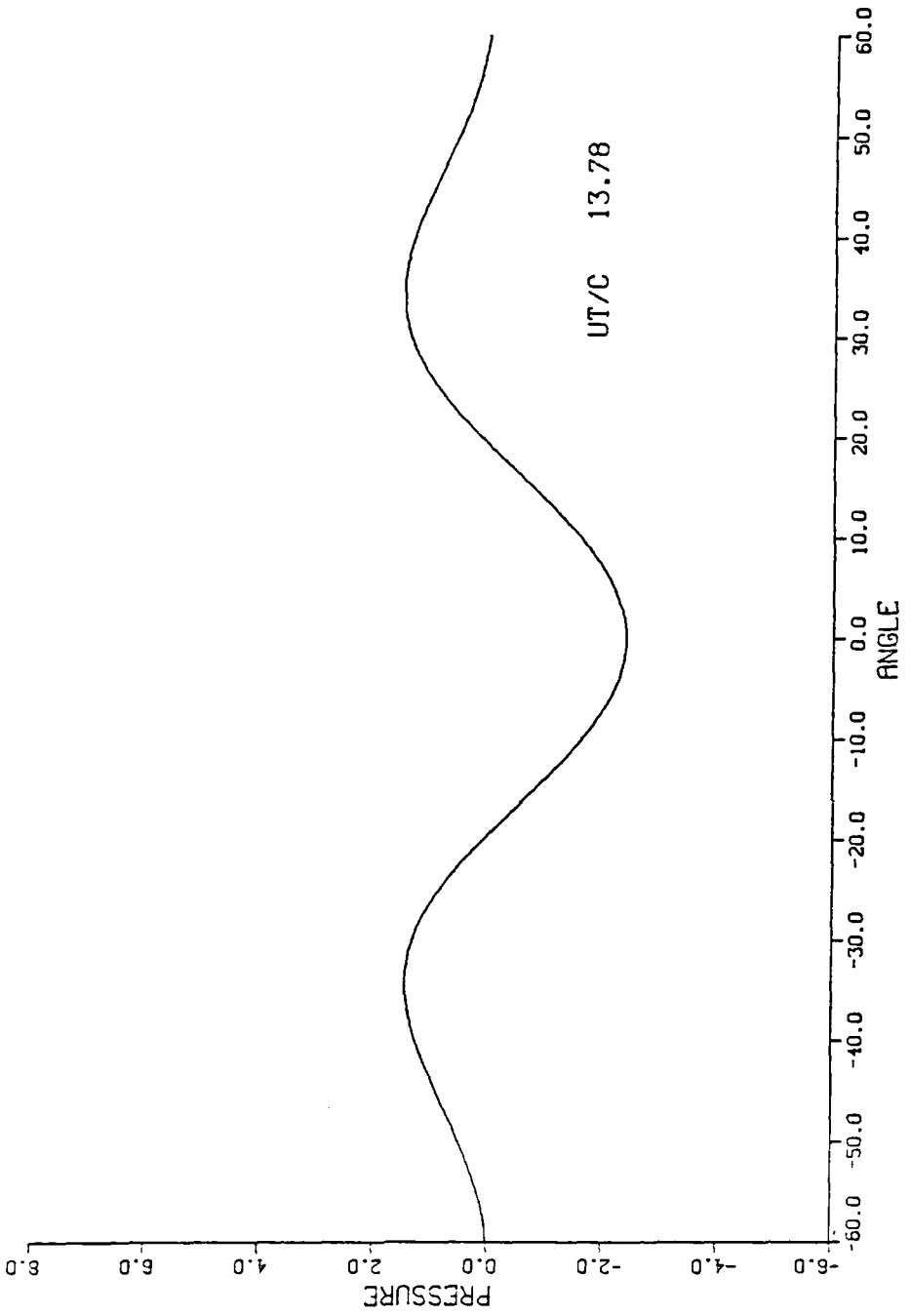

Figure 3.12 Differential pressure distribution at T* = 13.775

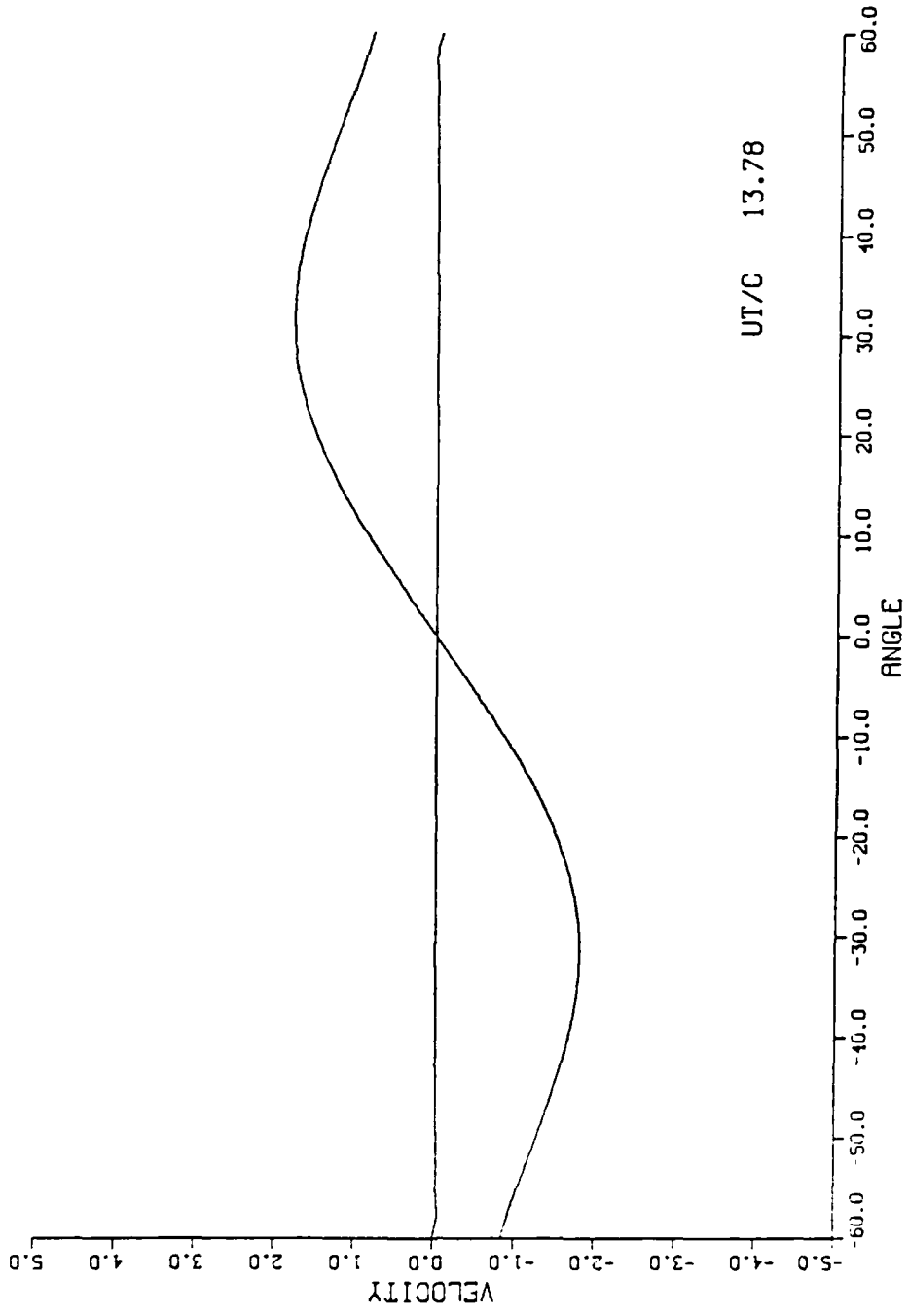

Figure 3.13 Velocity distribution on both faces of the camber at T* = 13.775

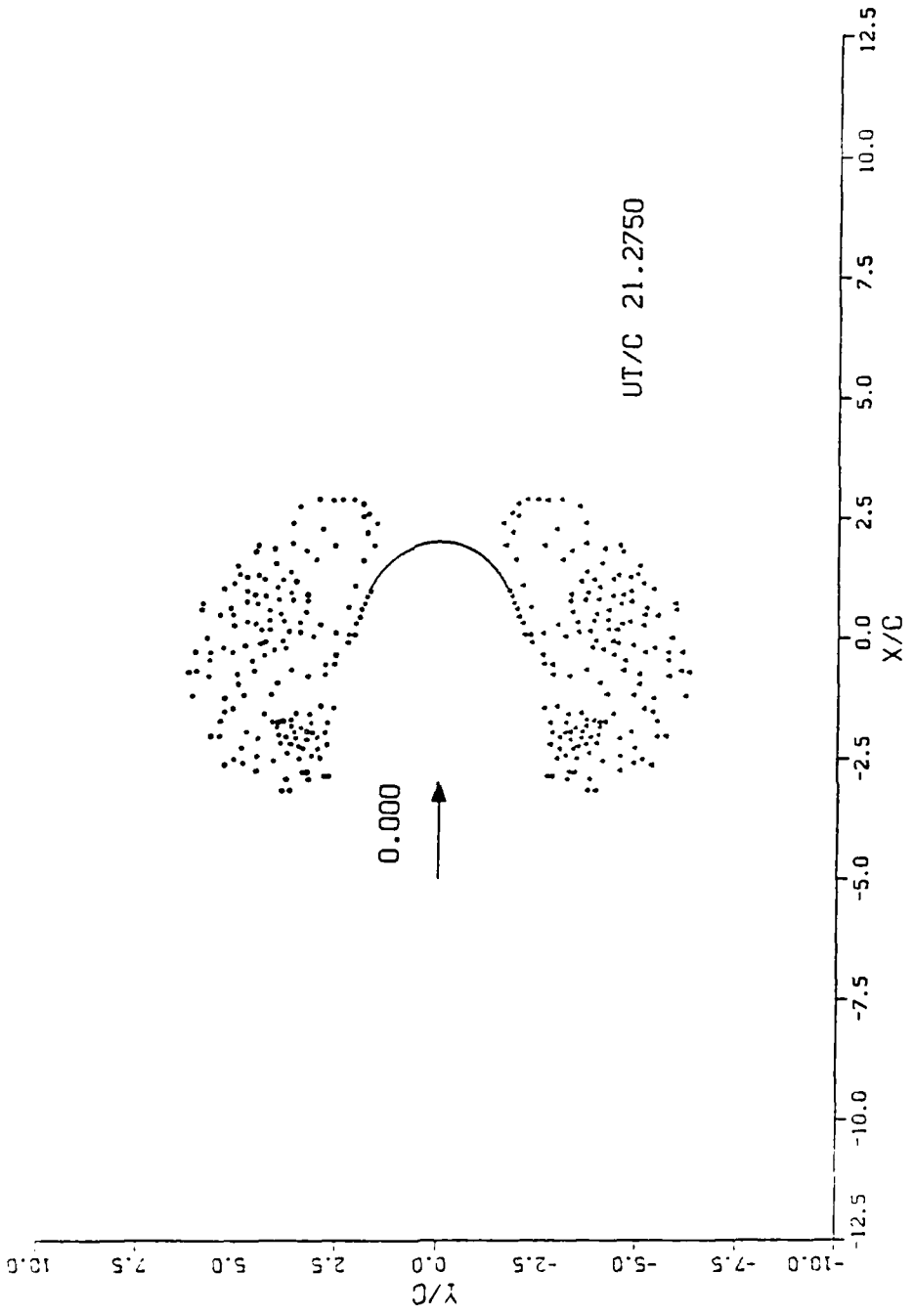

Figure 3.14 Position of vortices at T* = 21.275

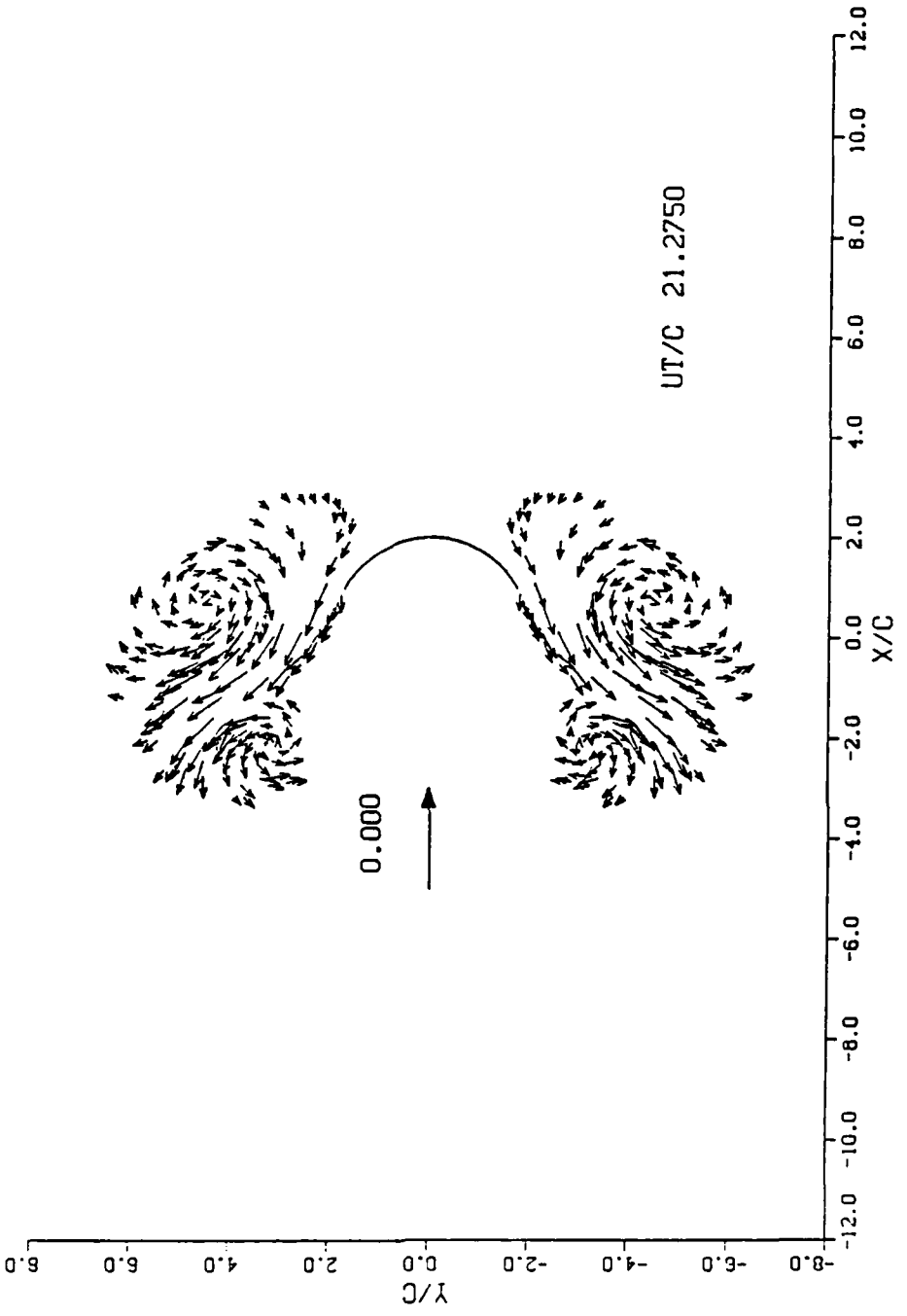

Figure 3.15 Instantaneous velocity of the vortices at T* = 21.275

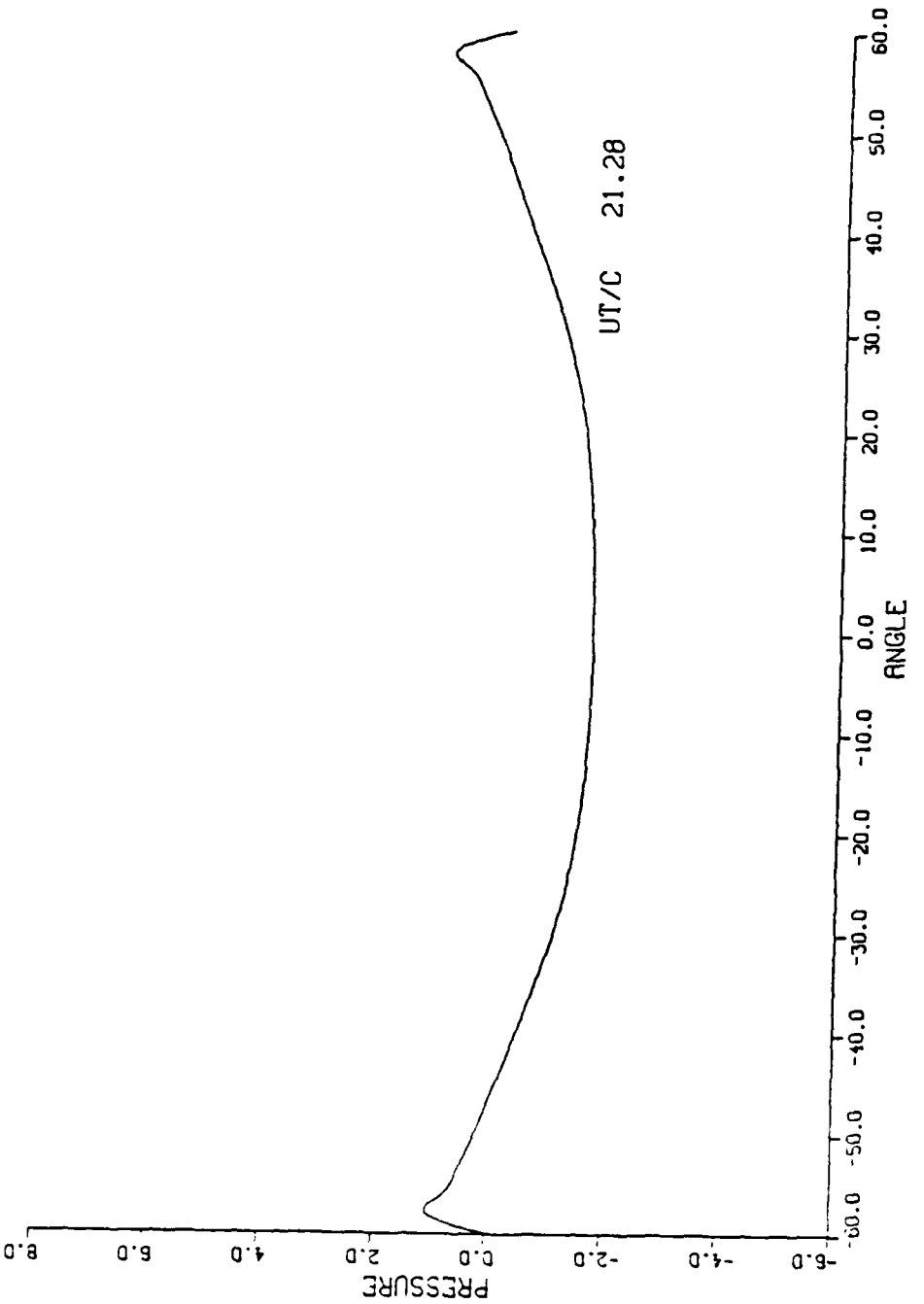

Figure 3.16 Differential pressure distribution at T* = 21.275

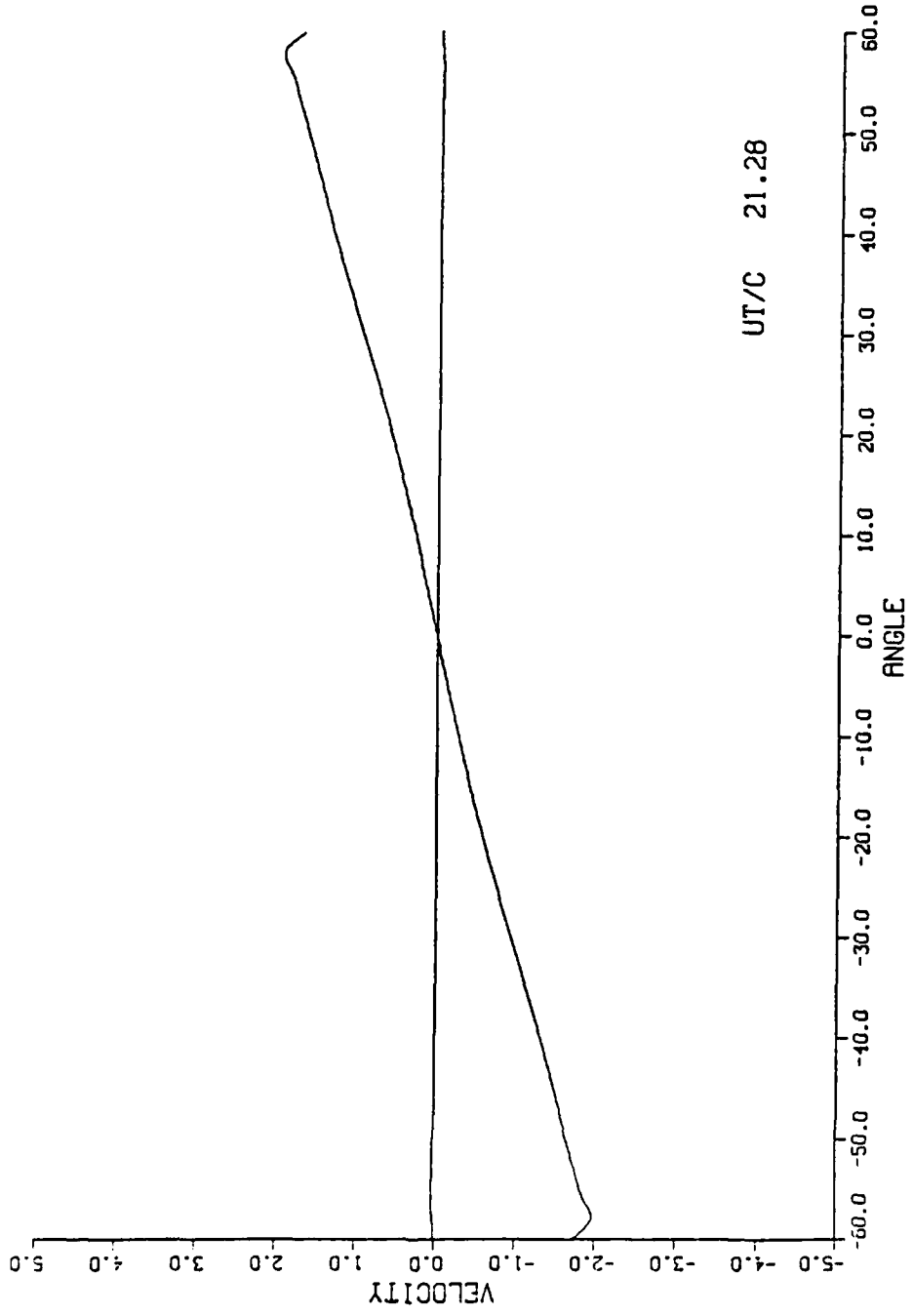

Figure 3.17 Velocity distribution on both faces of the camber at $T^* = 21.275$

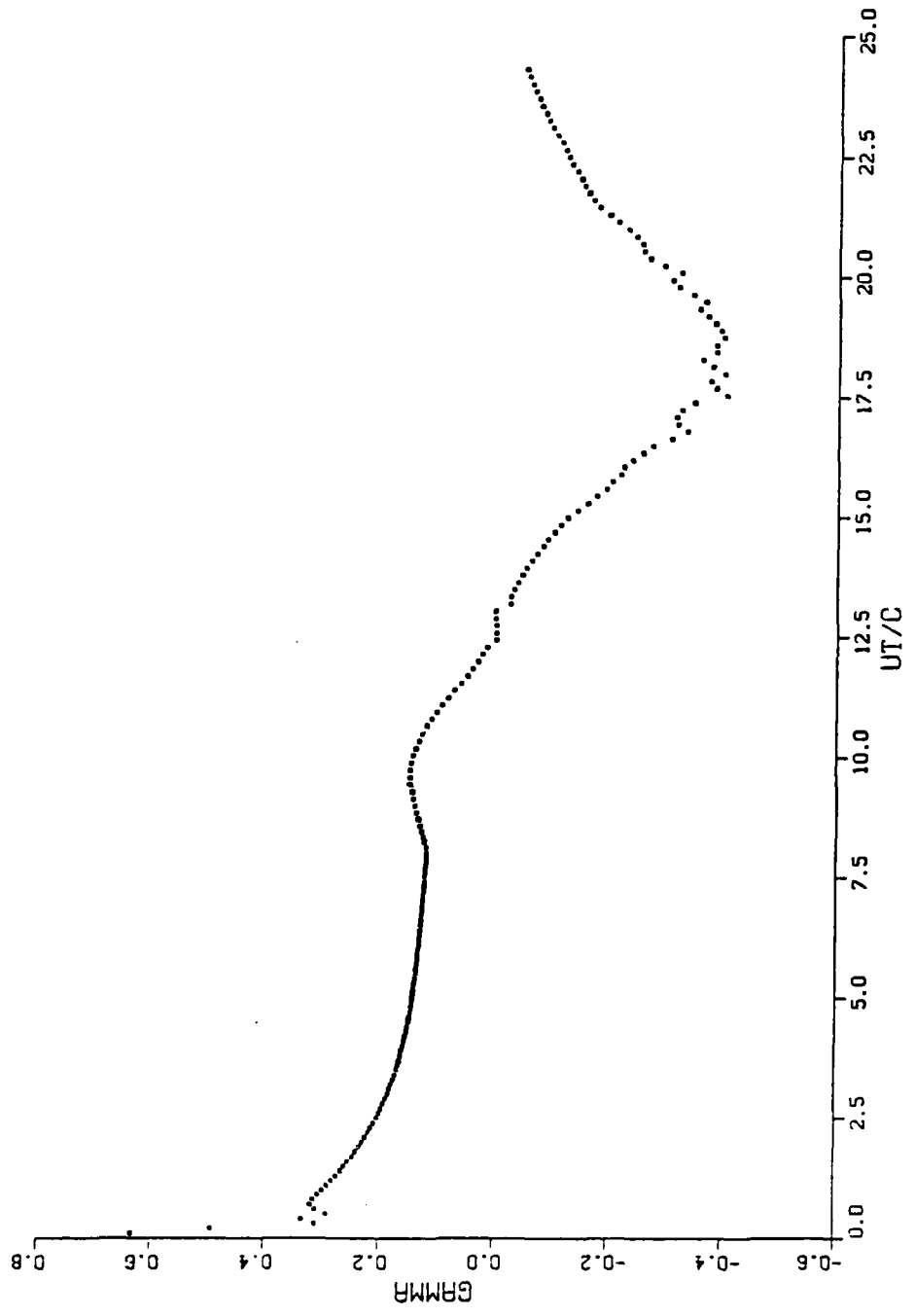

Figure 3.18 Variation of the circulation of the nascent vortex with T*

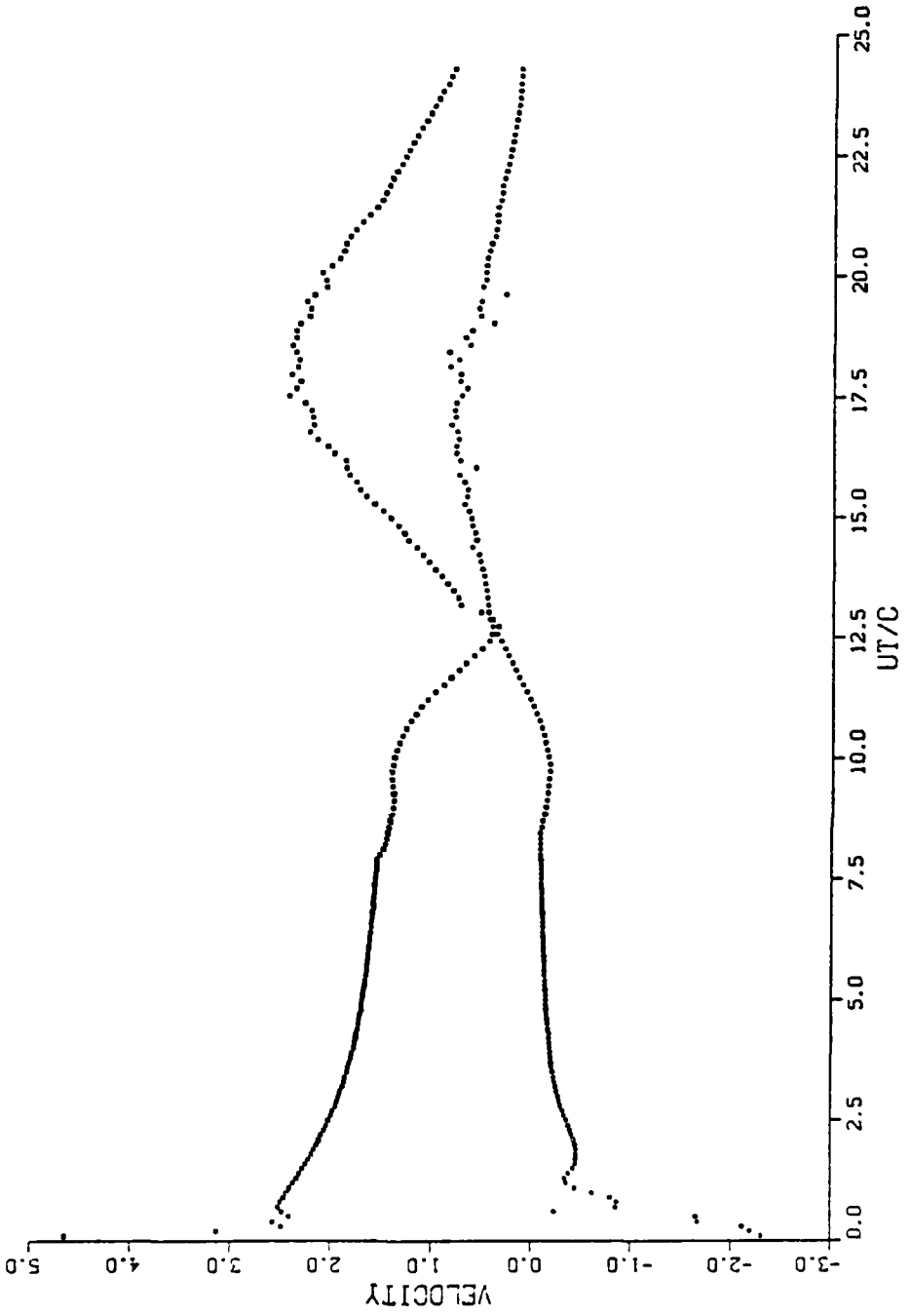

Figure 3.19 Variation of the velocities V_1 and V_2 with T*

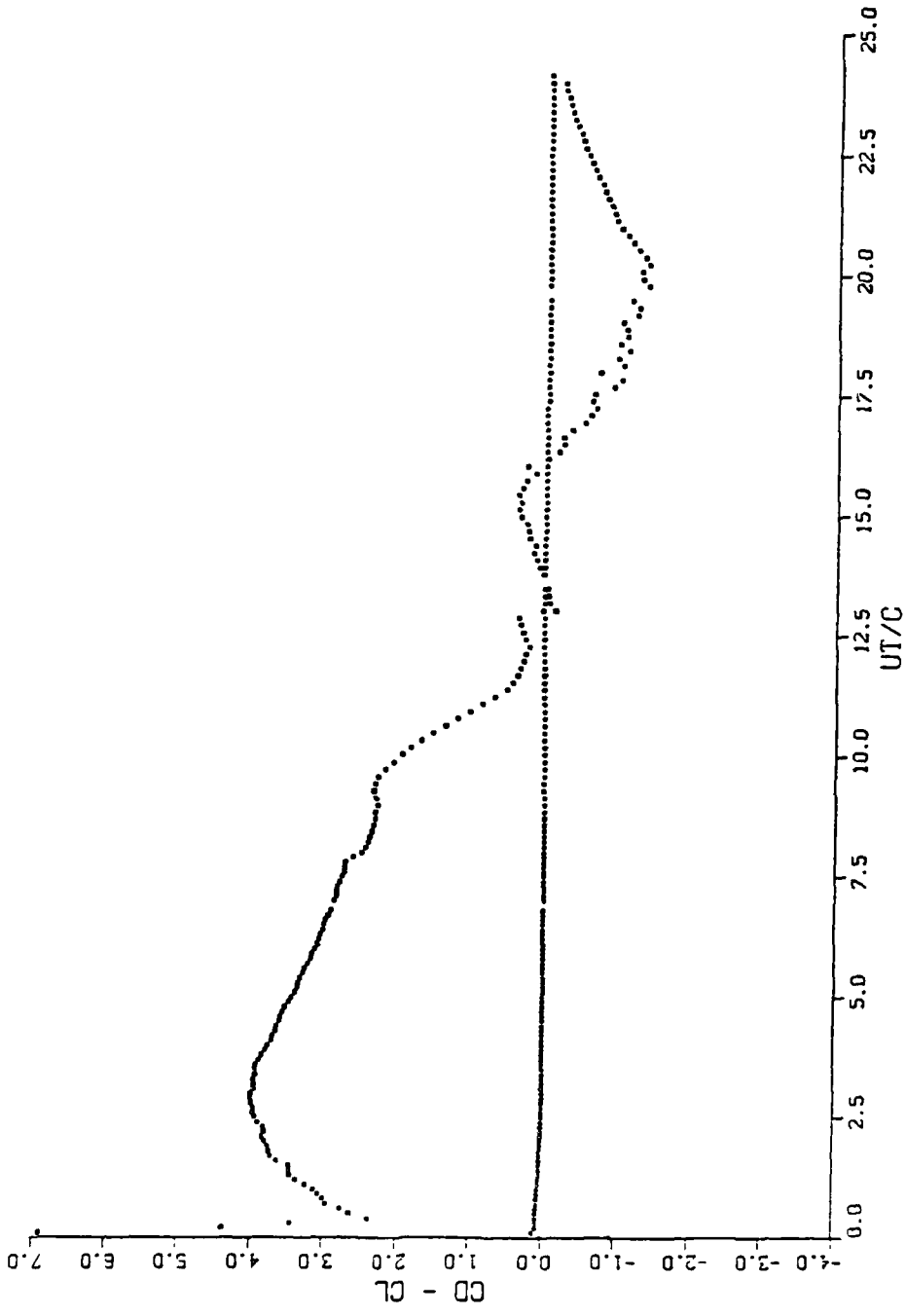

Figure 3.20 Calculated drag coefficient as a function of T*

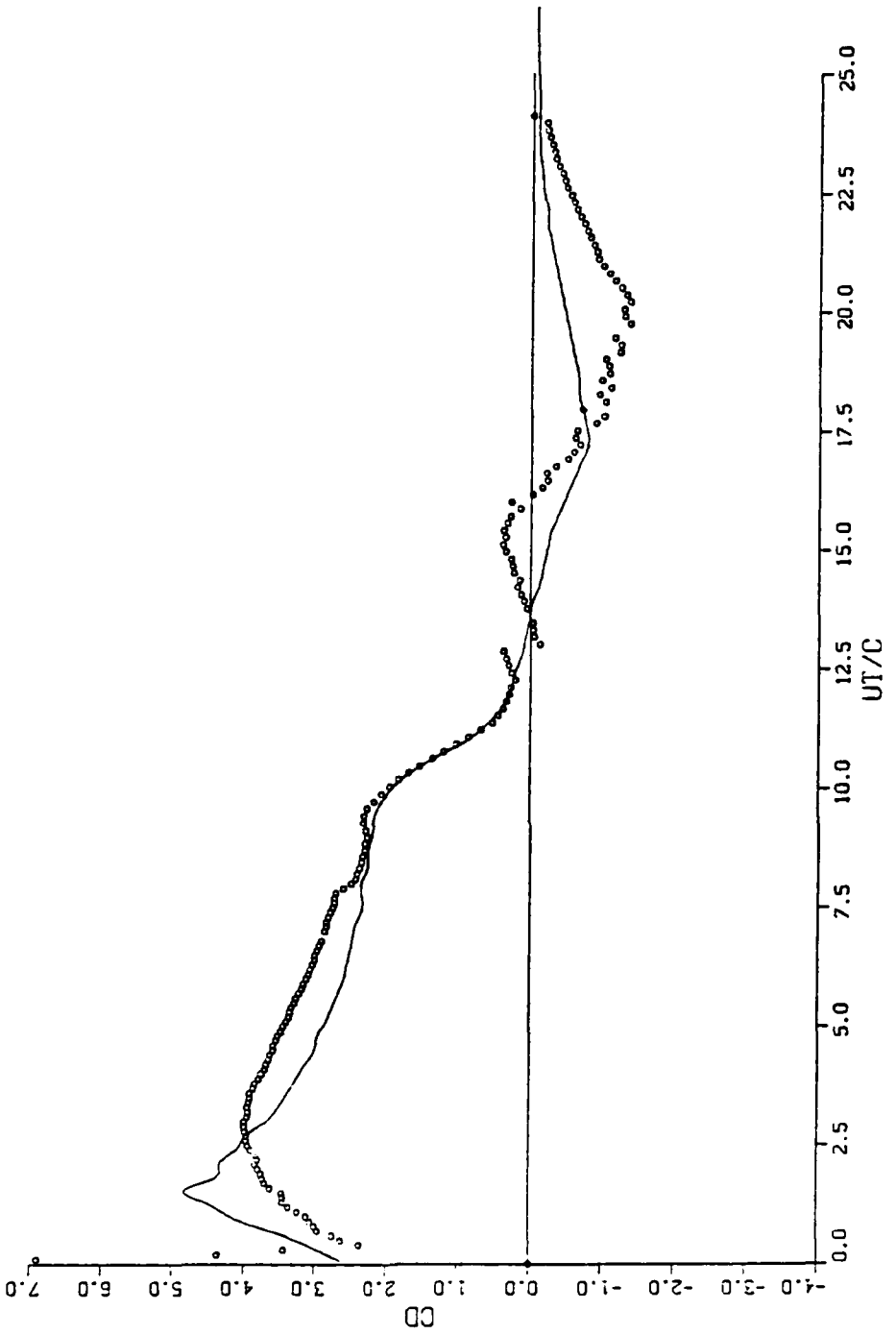

Figure 3.21 Comparison of measured and calculated drag coefficients

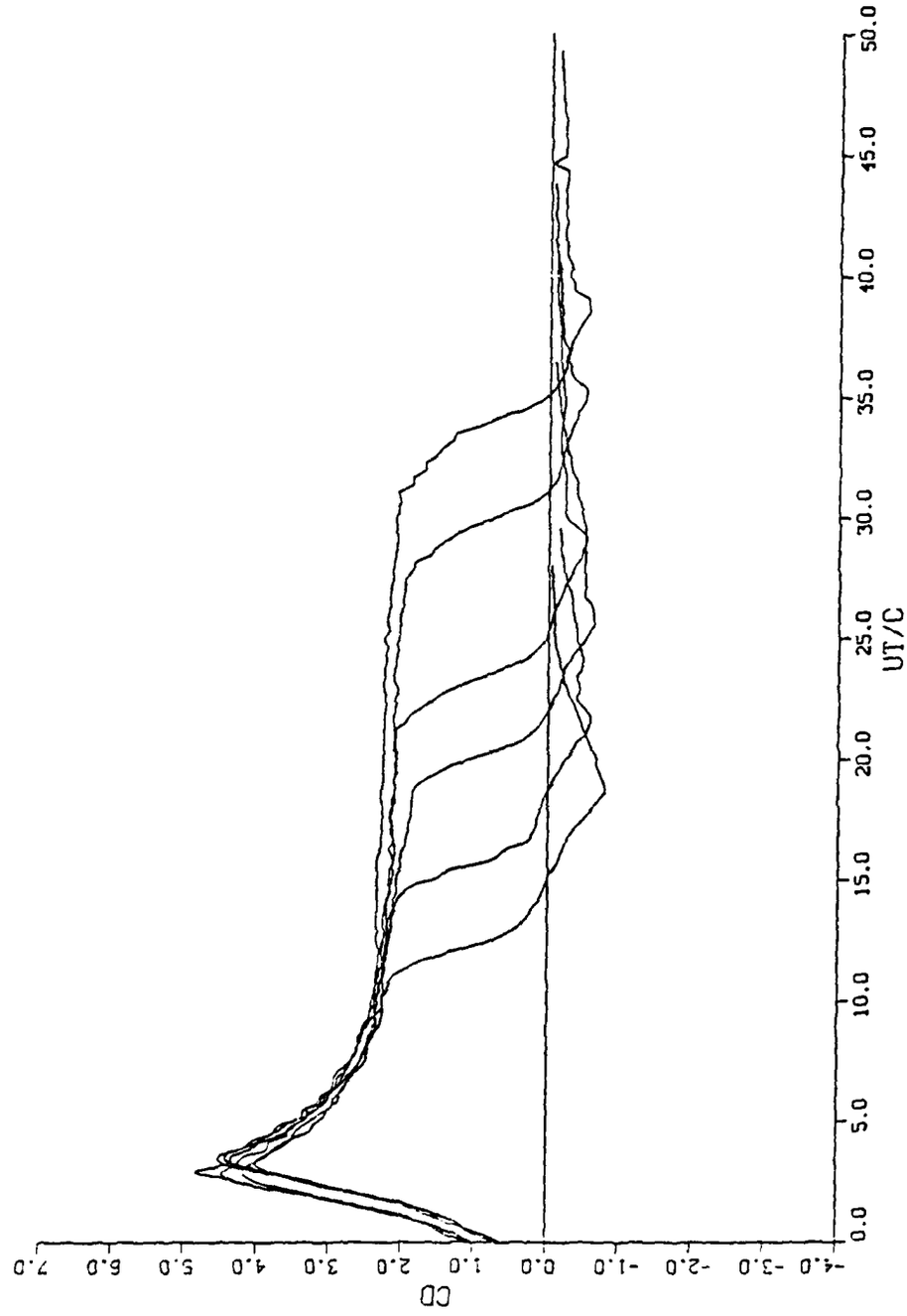

Figure 3.22 Measured drag coefficients for various periods of initial steady flow

B. CONCLUDING REMARKS

The results presented in this section have shown that the discrete vortex model can be used with confidence to predict the evolution of the wake about a cambered plate immersed in an arbitrary time-dependent flow. The drag coefficients resulting from the analysis and experiments agree reasonably well. This agreement can be improved with the introduction of a small circulation dissipation.

The development of negative differential pressures near the central region of the camber is thought to be primarily responsible for the inception of the partial collapse of a parachute at high rates of deceleration. This phenomenon takes place even when the total drag force acting on the parachute is still positive. The sample analysis presented herein also shows that the negative differential pressure can cover a large region of the parachute and even result in negative drag. The basic idea emerging from the analysis reported herein is that the designs which incorporate into them the idea of delaying or preventing the return of the shed vortices to the canopy (e.g.,porosity management, change of deceleration history, parachute shape, dissipation and or destruction of the organized wake) will be the ones which could avoid the collapse phenomenon. Extensive analysis and small scale experiments coupled with a few judiciously selected field tests may help to arrive at practically and phenomenologically sound parachute designs.

LIST OF REFERENCES

Chorin, A.J. 1973. "Numerical Study of Slightly Viscous Flow," *Journal of Fluid Mechanics* Vol. 57, pp. 785-796.

Clements, R. 1973. "An Inviscid Model of Two-Dimensional Vortex Shedding," *Journal of Fluid Mechanics* Vol. 57, pp. 321-335.

Fage, A. and Johansen, R. C. 1928. "The Structure of Vortex Sheets," *Aeronautical Research Council* R&M, No. 1143.

Heinrich, H. G. and Saari, D. P. 1978. "Parachute Opening Shock Calculations with Experimentally Established Input Functions," *Journal of Aircraft* Vol. 15, No.2, pp. 100-105.

Klimas, P. C. 1977. "Fluid Mass Associated with an Axisymmetric Parachute Canopy," *Journal of Aircraft* Vol. 14, No. 6 pp. 577-580.

McWey, D. F. and Wolf, D. F. 1972. "Analysis of Deployment and Inflation of Large Ribbon Parachutes," *Journal of Aircraft* Vol. 11, pp. 96-103.

Muramoto, K. K. and Garrard, W. L. 1984. "A Method for Calculating the Pressure Field about a Ribbon Parachute Canopy in Steady Descent," AIAA 8th Aerodynamic Decelerator and Balloon Technology Conference, Hyannis, Mass., AIAA-84-0794.

Mostafa, S. I. M. 1987. "Numerical Simulation of Unsteady Separated Flows," Ph.D. Thesis, Naval Postgraduate School, Monterey, California.

Sarpkaya, T. 1967. "Separated Unsteady Flow about a Rotating Plate," In *Developments in Mechanics* Vol. 4, pp. 1485-1499.

Sarpkaya, T. 1968. "An Analytical Study of Separated Flow about Circular Cylinders," *Journal of Basic Engineering* Trans. ASME, Vol. D-90, pp. 511-520.

Sarpkaya, T. 1975. "An Inviscid Model of Two-Dimensional Vortex Shedding for Transient and Asymptotically Steady Separated Flow over an Inclined Plate," *Journal of Fluid Mechanics* Vol. 68, pp. 109-128.

Sarpkaya, T., and Ihrig, C. J. 1986. "Impulsively Started Flow about Rectangular Prisms: Experiments and Discrete Vortex Analysis," *Journal of Fluids Engineering* Vol. 108, pp. 47-54.

INITIAL DISTRIBUTION LIST

		No. Copies
1.	Defense Technical Information Center Cameron Station Alexandria, VA 22304-6145	2
2.	Library, Code 0142 Naval Postgraduate School Monterey, CA 93943-5002	2
3.	Department Chairman,Code 69 Naval Postgraduate School Monterey, CA 93943-5000	2
4.	Prof. T.Sarpkaya Code 69SL Naval Postgraduate School Monterey, CA 93943-5000	6
5.	Dr. Samir I. M. Mostafa Department of Mechanical Engineering Naval Postgraduate School Monterey, CA 93943-5000	1
6.	Mr. Raymond J. Munz 39 Eagle Lane Hauppauge, NY 11788	1
7.	Mr. Adolf F. Muller 13 - 21st Ave. BayShore, NY 11706	1
8.	LCDR Paul D. Munz 39 Eagle Lane Hauppauge, NY 11788	5

END

10-87

DTIC